land

MDPI

Article

Spatio-Temporal Land-Use/Land-Cover Change Dynamics in Coastal Plains in Hangzhou Bay Area, China from 2009 to 2020 Using Google Earth Engine

Yinghui Zhao [1,2], Ru An [1], Naixue Xiong [3], Dongyang Ou [4] and Congfeng Jiang [4,*]

1 School of Earth Science and Engineering, Hohai University, Nanjing 210098, China; zhaoyinghui3319@163.com (Y.Z.); anrunj@163.com (R.A.)
2 Department of Water Resources, Zhejiang Tongji Vocational College of Science and Technology, Hangzhou 311231, China
3 Department of Mathematics and Computer Science, Northeastern State University, Tahlequah, OK 74464, USA; xiong31@nsuok.edu
4 School of Computer Science and Technology, Hangzhou Dianzi University, Hangzhou 310018, China; oudongyang@hdu.edu.cn
* Correspondence: cjiang@hdu.edu.cn

Abstract: Land-use classification is fundamental for environmental and water resource evaluation in coastal plain areas. However, comprehensive remote sensing image-based land-use analysis is challenged by the lack of massive remote sensing images and the massive computing power of large-scale server systems. In this paper, the spatial-temporal land-use change characteristics of the Hangzhou Bay area coastal plain are investigated on the Google Earth Engine platform. The proposed model uses a random forest algorithm to assist the land-use classification. The dataset is selected from the year 2009 to 2020 and classified with an average classification accuracy of 89% and Kappa coefficient of 88%. The results show that the land use in the selected region is affected by urbanization, the balance of cultivated land occupation and compensation, construction of economic development zone, and other activities. The investigation also shows that in the past 12 years, land use has changed rapidly, and each land-use type maintains the dynamic balance of occupation and compensation. Although the overall land-use distribution is stable, the information entropy fluctuates at a high level, with an average value of 1.15, and the multi-year average value of equilibrium is as high as 0.83. The driving force of land-use change is analyzed and accounted as demographics and human population dynamics, social-economic development, urbanization, and coupling effects of the above-mentioned factors.

Keywords: land use; coastal plain; spatial-temporal change; Google Earth Engine

Citation: Zhao, Y.; An, R.; Xiong, N.; Ou, D.; Jiang, C. Spatio-Temporal Land-Use/Land-Cover Change Dynamics in Coastal Plains in Hangzhou Bay Area, China from 2009 to 2020 Using Google Earth Engine. *Land* **2021**, *10*, 1149. https://doi.org/10.3390/land10111149

Academic Editors: Pere Serra and Marta Sapena

Received: 13 September 2021
Accepted: 27 October 2021
Published: 28 October 2021

1. Introduction

Land-use/land-cover (LULC) is usually defined as the human use of land, such as the economic and cultural activities (e.g., agricultural, residential, industrial, mining, and recreational uses) that are practiced at a given place. The rising human population and the associated demand for more land and natural resources are intensifying conflicts between human beings and wildlife worldwide. Land-use change is the result of the interaction between human beings and nature and has become one of the main reasons for global change at present. Land-use/land-cover changes can be made very frequently in both public and private lands due to very different uses. It seriously affects various fields closely related to human life, such as the ecological environment, economic development, food production, and climate change [1–5]. Land-use changes can also result in environmental changes due to the correlation of human activities and land-cover changes [6,7]. For example, nearly all waters contain dissolved salts and trace elements, many of which result from both the land use of human beings and the natural weathering of the Earth's surface.

Moreover, for agriculture, drainage waters from irrigated lands and effluent from city sewage and industrial wastewater can impact water quality. These are both examples that land use may have an impact on systematic environmental parameters changes.

Land-use/land-cover in public or private land both changes continuously and at many scales, from regional, national, to international scales. Land-use change also represents the regional, national, or international transition on human activity-based land-cover change. Specifically, land use can have specific and cumulative effects on air and water quality, watershed function, generation of waste, extent and quality of wildlife habitat, climate, and human health; therefore, land-use/land-cover change is a good indicator for natural, environmental, and social-economic development evaluation and sustainable development. Land use is also a secondary indicator for various evaluation and analysis, such as soil moisture deficit, drought impact on ecosystems, imperviousness and imperviousness change, vegetation productivity, landscape fragmentation pressure and trends, land take, land recycling, and densification. The dynamic changes of regional land use can effectively reflect the characteristics of land resources [8–11]. For example, Drummond et al. [12] proposed remote sensing data, statistical sampling, and change-detection-based approach to investigate how land conversion varies spatially and temporally across the east from 1973 to 2000, and how those changes affect regional land-change dynamics in the Eastern United States. The results show that agricultural land use has continued to decline, and that this enables forest recovery; an important land-cover transition has occurred, from a mode of regional forest-cover gain to one of forest-cover loss caused by timber cutting cycles, urbanization, and other land-use demands. Similarly, Wang et al. [13] proposed a land change detection method to capture significant land change hotspots over Northern China during 2001–2013, and further analyzed temporal trends and spatial patterns of LCLUC based on classification of annual LCLU maps from MODIS satellite imagery. The results provide the magnitude, trend, and spatial pattern of land-cover/land-use changes (LCLUC) to understand the mechanisms of LCLUC and assist land-use planning and conservation. In view of the contradiction between regional economic development and water environmental protection, the characteristics of the dynamic evolution of regional land use are analyzed, providing a scientific basis for further land-use planning and adjustment, and contributing to the formulation and implementation of local economic and environmental policies. Therefore, understanding the land-use evolution trend in coastal plains would support future regional planning toward providing disaster mitigation and appropriate land-use pattern planning. It may also help identify the ecological or disaster vulnerabilities in advance in coastal plains.

However, the dynamic analysis of spatial and temporal changes of land use cannot be separated from large-scale and periodic monitoring methods. Geographic information systems (GIS) and remote sensing (RS) can provide continuous and abundant data, and have the advantages of dynamic perception, fast operation, and macro analysis, which have already become the most effective means to obtain land-cover information [14,15]. With the development of scientific research, the demand for high-precision land-use data with continuous time and space is increasingly urgent. The explosion of geospatial data fundamentally changed human perception and interaction with the Earth; however, comprehensive remote sensing image-based land-use analysis is challenged by the lack of massive remote sensing images and the massive computing power of large-scale server systems. Fortunately, Google Earth Engine (GEE) platform has massive remote sensing data sets and large-scale spatial calculation and analysis functions, which can be used as an ideal platform to study the temporal and spatial changes of land use.

The fluvial and coastal landforms in the coastal plain have important roles in causing natural disasters and influence the water resource quality and environmental ecology evaluation under the expansion of land-use changing in the Hangzhou Bay Area in China. To improve the spatial-temporal resolution of ground object classification, this paper adopts the multi-temporal remote sensing data fusion classification and extraction technology based on the Google Earth Engine cloud platform and selects the Landsat 5 and Landsat

8 multi-temporal remote sensing image data with a high spectral and spatial resolution to obtain the dynamic evolution information of land use in the study area from 2009 to 2020. By analyzing the characteristics and influencing factors of land-use evolution in the past 12 years and discussing the correlation between land-use change and urbanization, economic development level, and industrial structure adjustment, this paper reveals the internal relationship between land-use change and social development.

Land-use/land-cover classification is a fundamental process to evaluate the present and the past land-use trend in targeted regions. There are two major approaches to classify the remote sensing images: supervised and unsupervised classification, while the latter also requires substantial input from the analyst. Land-use characterization is traditionally performed with field surveys or manual photo interpretation; both are time-consuming and labor-intensive. The accuracy of land-use classification depends on the amount of effort put in as well as the quality of the ground truth data against which the classification is judged. In this paper, the spatial-temporal change characteristics of coastal plain land use are investigated, where the spectral features and texture features of the ground surface are taken as the input parameters of the classifier to build a model, and the land is divided into four categories: water body, construction land, forest land, and cultivated land.

The purpose of this study was to analyze the spatial-temporal change characteristics of coastal plain land use in Hangzhou Bay Area on Google Earth Engine through big data analytics. Data were collected from various sources in Zhejiang Province, China, including the Department of Water Resources, Department of Natural Resources, Department of Marine Fisheries, local firms, meteorology, climatology observation data, and other local administrative agencies. The proposed model uses a random forest algorithm and sets the number of decision trees to 500 to assist the land-use classification. Through training the sample set, the land-use information of the northern plain area of Cixi City, Hangzhou Bay area, China from the year 2009 to 2020 was extracted, and nine periods of land-use data were obtained, with an average overall classification accuracy of 89% and Kappa coefficient of 88%. The results show that the land use in this region is affected by urbanization, the balance of cultivated land occupation and compensation, construction of economic development zone, and other activities. The investigation also shows that in the past 12 years, land use has changed rapidly, and each land-use type maintains the dynamic balance of occupation and compensation. Although the overall land-use distribution is stable, the information entropy fluctuates at a high level, with an average value of 1.15, and the multi-year average value of equilibrium is as high as 0.83. The complexity of land use is relatively high, while the dominance of dominant land types is relatively low. The driving force of land-use change is analyzed and accounted as demographics and human population dynamics, social-economic development, urbanization, and coupling effects of the above-mentioned factors. The result analysis also shows that the overall land use is disordered, with obvious traces of tidal flat reclamation and development, a high degree of land resources development, and frequent land-use transformation.

The paper is organized as follows. In Section 2, we describe the remote sensing data of the research area. In Section 3, we describe the land-use classification based on a random forest algorithm. We provide the classification results and precision in Section 4. In Section 5, we provide a comprehensive analysis of spatial-temporal change characteristics of land use of the researched coastal plain. The related work is presented in Section 6, and we conclude the paper with some future research directions in Section 7.

2. Study Area and Data Description

Hangzhou Bay area is located in the northeast of Zhejiang Province, bordering the Qiantang River in the west and the East China Sea in the east. It is a trumpet-shaped estuary formed by the Qiantang River entering the sea, and it is also a world-famous estuary known for its strong tide. The north bank of Hangzhou Bay is an erosive coast, while the south bank is a silting coast. This study area is presented in Figure 1, which is on the south bank of Hangzhou Bay and belongs to the coastal plain in the north of Cixi City.

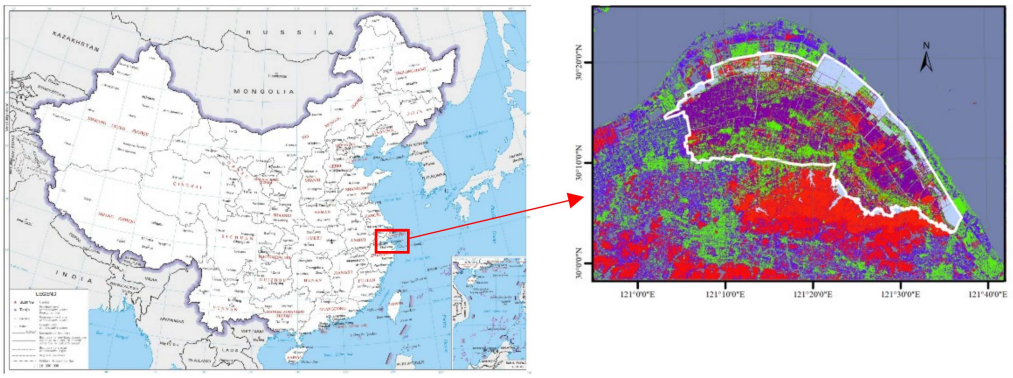

Figure 1. Location of research area.

In the upper-right figure of Figure 1, the white outlined area is the research area where different color means different land use/land cover; specifically, red means construction land, green means forests, purple means cultivated land, and gray means water body.

It is adjacent to Zhenhai City, Ningbo in the southeast, Yuyao City in Shaoxing in the southwest, and protrudes into Hangzhou Bay in an arc shape in the north. Its geographical coordinates are between 30.2–30.21 north latitude and 121.2–121.38 east longitude, with a total area of 862 km^2, as shown in Figure 1. The coastline starts from the tidal flat junction of Yuyao City in the west and ends at the tidal flat junction of Cixi City and Zhenhai district in the east. It is an artificial coastline with a total length of 72.4 km and a first-line seawall with a total length of 72.4 km.

GEE platform can provide Landsat satellite time-series image data covering the study area. With its advantages of parallel operation and quick analysis, the time series distribution map of land-use change in the study area can be extracted. In this paper, 2009-2020 is selected as the target year of land-use change in the study area, and the minimum cloud amount image in each target year is selected as the original image, thus increasing the accuracy of classification.

The data of 2009, 2010, and 2012 were provided by the Landsat-7 satellite, which carried an Enhanced Thematic Mapper (ETM+) sensor, with eight bands and a scanning band width of 185 km. The data from 2013 to 2020 were provided by the Landsat-8 satellite, which is equipped with an OLI (Operational Land Imager) land imager with nine bands and TIRS (Thermal Infrared Sensor) thermal infrared sensor with two bands. The coverage of one scene is 185 km wide. According to the different application range of each band of the sensor, to highlight the features of ground objects and improve the ability of visual interpretation, this paper selects the Landsat-7 satellite bands five, four, and three and Landsat-8 satellite bands six, five, and four for color synthesis, which makes it easy to distinguish the types of objects in the image; therefore, it is beneficial to the extraction of land-use/cover information. The study area belongs to the coastal plain, which is flat, and the influence of topographic features is not considered. Auxiliary data include regional digital maps, river system survey maps, urban planning data, and statistical yearbooks of the most recent 12 years. Road, water system, and urban planning information are combined with field survey data analysis, which is mainly used for the correction of classification results and accuracy verification.

Landsat 7 ETM+ SLC-off data refer to all Landsat 7 images collected after May 31, 2003, when the Scan Line Corrector (SLC) failed. Although these products have data gaps, they are still useful and maintain the same radiometric and geometric corrections as data collected prior to the SLC failure. We apply the patching approach from USGS to preprocess the EMT+ data in our study [16].

3. Research Method

In this study, we collected the social and economic data of the research area from 2009 to 2020 and investigated the driving force of land-use change in the target area

based on the primary component analysis approach. In order to compare the land-use change and its trend in different years, we selected 9 parameters from the yearbook of the municipal government, such as the annual residential population and its proportion in country and urban areas, regional gross product, gross product of agriculture (primary industry), gross product of the industrial sector, i.e., the secondary industry, including mining, manufacturing, electricity, construction, and utility sectors, gross product of service sector, total electricity usage, and electricity usage of the industrial sector. Then, we used the 9 parameters to build our driving force model for the research area, integrating the factors from different dimensions, such as population, economic development, agriculture, forest industry, construction industry, etc. In the following sections, we describe our research methodology more specifically.

We demonstrate the flowchart of our methodology for GEE-based LULC classification and change analysis in Figure 2.

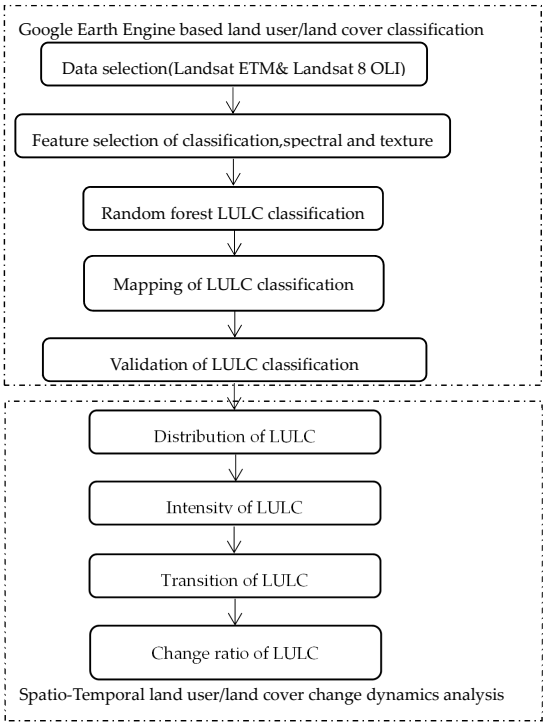

Figure 2. Flowchart of GEE-based LULC classification and change analysis.

3.1. Data Acquisition

According to the actual land-use situation in the study area, the land-use types are divided into four categories: water, construction land, forest land, and cultivated land. The land-use classification scheme is shown in Table 1.

Table 1. Land-use classification scheme.

ID	Land Type	Feature
1	Water	Natural land waters and land for water conservancy facilities
2	Construction land	Urban and rural residential areas and industrial, mining, transportation, and other land
3	Forest	Natural forest and plantation with canopy density more than 15%. It includes timber forest, economic forest, and shelter forest.
4	Cultivated land	Farmland that can be cultivated normally in ordinary years.

These four types of first-class features can be distinguished and have obvious characteristics in remote sensing images. The minimum cloud cover image of each target year in the study area was selected as the data source to establish the sample data set. After radiation correction, the images were cut and spliced, and then the bands were synthesized.

The sample data set constructed from 2009 to 2020 was selected as the classification data in the study period—no data meeting the conditions were obtained in 2011, 2013, and 2018. The data in 2009, 2010, and 2012 were Landsat-7 images, and the data in other years were Landsat-8 images. The image with 0% cloud cover in the first period of that year was selected as the sample.

Taking Landsat-8 image data in 2020 as an example, firstly, the high-resolution image provided by GEE was used for visual interpretation, and the sample data of four different land-use types in the study area were selected. In Google Earth, the selected sample points were checked and corrected according to the distribution of features in the study area and the field survey results, and the sample data set of 2020 was established, which was used as the standard data reference system to establish the sample data set of other years. The sample data of other years were tested and discriminated according to the features of features change and prior knowledge in the study area. Among them, there were 50 samples for water classification, 100 for construction land, 100 for forest land, and 100 for cultivated land. Finally, 80% of the sample data of each period was used as the training samples of the classifier for classification, and the remaining 20% was used for accuracy evaluation.

3.2. Feature Sets Construction of Land-Use/Land-Cover Classification

Based on GEE, spectral features and texture features of the ground surface were extracted as input parameters of the classifier.

In remote sensing images, the spectral features are the spectral distribution and gray scale of target objects or the brightness ratio between bands. To reduce the amount of data calculation and improve the calculation speed, it is necessary to make full use of the spectral characteristics of images. Considering the band characteristics and application range of the images, as well as the recognition characteristics of ground objects in visible light, the bands 1, 2, 3, 4, 5, and 7 of Landsat-7 ETM+ images and bands 2, 3, 4, 5, 6, and 7 of Landsat-8 OLI images are selected as the multispectral classification feature data.

Water and vegetation are the two main components of land cover, and the impenetrable water surface composed of houses, roads, and other buildings is the most direct embodiment of human influence on the environment. To highlight the information of water, vegetation, and artificial surface, it is necessary to extract spectral index. In this paper, an improved modification of the normalized difference water index (*MNDWI*) is introduced. Normalized difference vegetation index (*NDVI*) and normalized difference built-up index (*NDBI*) can be used to distinguish water, vegetation, and impervious surface. Taking Landsat-8 OLI sensor data as an example, the expression of three exponents is as follows:

$$MNDWI = \frac{B3 - B6}{B3 + B6} \tag{1}$$

$$NDVI = \frac{B5 - B4}{B5 + B4} \tag{2}$$

$$NDBI = \frac{B6 - B5}{B6 + B5} \tag{3}$$

Due to the significant spectral characteristics of water, it has strong absorption in the infrared band and weak absorption in the visible band, and its spatial geometry and texture features are easy to identify, so the interpretation of water is relatively simple in many land types. Based on spectral classification and referring to the research results of the Cixi water area investigation report over the years, the water body classification results are revised to improve the accuracy of water body information extraction and ensure the accuracy of classification results.

After the water body is identified with high precision, it is necessary to interpret and separate the building land. *NDVI* and *NDBI* are used to distinguish vegetation from buildings. *NDVI* is used to describe the growth state and coverage of plants, and the value range is [−1,1]. The larger the value, the more likely the land belongs to vegetation. *NDBI* is often used to interpret buildings, and its value range is also [−1,1]. The larger the value, the greater the possibility that the plot is a building. The spectral characteristics of cultivated land, garden land, and forest land are not obvious.

As a regional feature in an image, texture features change with scale, and its extraction is closely related to the size of the region. The grey-level co-occurrence matrix (GLCM) reflects the gray-level changes of adjacent pixels in a specific area or two pixels at a certain distance in an image, which can be used to study the spatial correlation characteristics of gray level, and then to count texture features. By calculating the gray-level co-occurrence matrix, many texture features can be obtained to assist remote sensing image classification. In this paper, the statistical texture method based on the gray-level co-occurrence matrix is used to calculate, while entropy, contrast, angular second moment and correlation, are used to extract the image texture features. The classification feature set is shown in Table 2.

Table 2. Classification feature collection.

Feature	Data Source	Band
Spectral features	Landsat-7 multi-Spectrum Image Bands	*B*1, *B*2, *B*3, *B*4, *B*5, *B*7
	Landsat-8 multi-Spectrum Image Bands	*B*2, *B*3, *B*4, *B*5, *B*6, *B*7
	Spectrum Index	*MNDWI*, *NDVI*, *NDBI*
Texture features	GLCM	Entropy, Contrast, Angular Second Moment and Correlation,

3.3. Land-Use/Land-Cover Intensity Quantification

In this paper, the main processes involved in the calculation and analysis of land-use change in the study area are preprocessing and standardization of minimum cloud image data, the establishment of a classification feature set, classification by random forest algorithm, and accuracy evaluation. Based on GEE, these methods use a supervised classifier algorithm, Landsat observation data of each target year, and independently compiled programs to map and evaluate land-use distribution. To analyze the changes more accurately in the land-use distribution in the study area, information entropy, equilibrium, and dominance are used to evaluate the changes in land-use distribution.

The concept of entropy originates from thermo-physics, and information entropy is a concept used to measure the amount of information in information theory. The more orderly a system is, the lower the information entropy is. On the contrary, the more chaotic a system is, the higher the information entropy is; therefore, information entropy is also a measure of the degree of system order. The greater the uncertainty of a variable, the greater the entropy, and the greater the amount of information needed to make it clear. Information entropy is used to measure the order and complexity of land-use types, that is, the diversity of landscapes. The calculation formula is as follows:

$$H = -\sum_{i=1}^{n} p_i ln(p_i) \quad (4)$$

In the above formula, H represents the information entropy value, i represents various land-use types, n represents the number of land-use types, and p_i represents the area percentage of various land-use types. The smaller the entropy value, the higher the order degree of land-use distribution, and the higher the entropy value, the lower the order degree of land-use distribution. When there is only one land-use type in the study area, the information entropy value is the smallest $H = 0$. When the proportion of various

land-use types is equal, H reaches the maximum value, and it is expressed as $H_{max} = ln(n)$. Information entropy also reflects the diversity of land-use types.

Based on information entropy, the concept of equilibrium degree is established to measure the homogeneity and equilibrium of land-use distribution, and the expression of equilibrium degree is shown in Equation (5):

$$J = H/H_{max} = -\sum_{i=1}^{n} p_i ln(p_i)/ln(n) \quad (5)$$

In Equation (5), J represents the equilibrium degree, $J \in [0,1]$. The greater the value of J, the stronger the equilibrium degree and the higher the complexity of land-use distribution. When $J = 1$, land use reaches the highest equilibrium state, and the uniformity of patch distribution of each land-use type reaches the maximum. Corresponding to it is dominance, as shown in Equation (6):

$$I = 1 - J \quad (6)$$

In Equation (6), I represents dominance, which is opposite to equilibrium and reflects the concentration of land use, i.e., the degree to which one or several dominant land types dominate the land types in the region.

Patch density represents the number of patches per unit area, and the calculation is listed as follows:

$$PN = \frac{N}{A} \quad (7)$$

In Equation (7), n is the total number of patches in the study area, and a is the total area of the study area in km^2.

To compare the differences and changing trends of different land-use types, this study quotes the dynamic attitude of land use to quantitatively reflect the changing rate of land-use types through the dynamic attitude of a single land-use type. The dynamic attitude of land use refers to the change rate of a certain type of land area in a period, and its expression is listed in Equation (8):

$$K_i = \frac{U_b - U_a}{U_a \times T} \quad (8)$$

In Equation (8), K_i is the dynamic attitude of a land-use type in t period. U_a and U_b are the areas of a certain land-use type at the beginning and end of the study. T is the research period, which is the annual change rate of a land-use type when expressed in years.

To further reflect the complexity of landscape spatial structure and the degree of human disturbance to landscape, it is necessary to calculate the fragmentation index of different land-use types, that is, the fragmentation degree of the land-use landscape. The original natural landscape is generally closer to a single, homogeneous, and continuous whole. However, under natural or human disturbance, the land-use type gradually tends to be complex, heterogeneous, and discontinuous patch mosaic, and the change of fragmentation degree of land use can directly reflect the interference degree of land use. The formula of land-use fragmentation is as follows:

$$C_i = N_i/A_i. \quad (9)$$

In the above formula, C_i is the fragmentation degree of land-use type I, N_i is the patch number of land-use type I, and A_i is the total area of land-use type i.

Land-use intensity includes the breadth and depth of land use. To reflect the development and utilization of land resources by human beings, it is necessary to express land-use

intensity quantitatively. The comprehensive index of land-use intensity change is used to describe the amount and rate of land-use change, and its expression is listed as follows:

$$L = 100 \times \sum_{i=1}^{3} A_i \times C_i \quad (10)$$

In Equation (10), L is the comprehensive index of land-use intensity, A_i is the I-level land-use intensity classification index, and C_i is the percentage of the I-level land classification area.

3.4. Classification Based on Random Forests Algorithm

The main parameters of a random forest classifier based on GEE include the number of classification trees, the number of variables of each classification tree, the minimum sample leaves, the input variables of a decision tree, OOB mode, and the random seed variables used to construct a decision tree. The random forest algorithm uses random sample data to generate multiple decision trees independently. The best node of each decision tree depends on the randomly selected subset of prediction variables, and the number of decision trees depends on the number of prediction variables [17]. When the number of decision trees increases, the overall accuracy of classification increases. The optimal parameter values are selected by the selected training samples. After the random forest algorithm runs, the overall accuracy, producer accuracy, and user accuracy are obtained by a confusion matrix to verify the classification effect. The pseudo-codes of the proposed algorithm are listed in Algorithm 1.

The goal of classification is not only to obtain higher overall classification accuracy, but also to ensure that the minimum missing error and the minimum wrong error are in a more appropriate range. More sample quantity and sample purity of ground objects are beneficial to obtain higher classification accuracy. The result of supervised classification depends on the input training samples. To accurately distinguish the ground objects in different environments and conditions, many samples are needed as the initial data set to train the classifier in complex areas.

To ensure the accuracy of classification, a large sample size is needed. In this paper, an iterative sample selection program is introduced to train the machine learning algorithm. Firstly, the existing training samples are used to construct the random forest classifier, and the random forest algorithm is used to classify the selected image set based on the GEE platform. Then, the classification results are visually evaluated and compared by referring to the electronic map of the study area and the five-meter-high resolution image in Google Maps. For the more difficult positions, the training data set is further expanded until the classification becomes stable. The initial classification count starts from 40 samples, and the sample size is gradually increased. After each iteration, the classification results are compared with the sub-meter high-resolution images. If the classification results are not satisfactory, the training samples are added until the satisfactory classification results are obtained (the classification accuracy is higher than 85%).

Algorithm 1 Random-Forests-Based Land-Use Classification

Input: ***landDataSet***: Land-use dataset and image set
totalDecisionTree: number of total decision tree
minSplitThreshold: the minimum split threshold
F: Land-use feature dimension
Output: LUCM: ***land-use classification model***
trainSet, testSet = RandomSplit(landDataSet, randomState=10)
for i in (1,2, . . . ,totalDecisionTree):
$D_i = Bootstrap(trainSet)$ // generating training data set D_i of each decision tree based on re-sampling
$rootNode_i = MakeNode(D_i)$ // generating the root node of the i*th* decision tree root node
$nodeQueue = Insert(rootNode_i)$ // adding the root node into the node queue
while $(not\ Empty(nodeQueue))$: // traverse the nodes to guarantee enough growth of the decision tree.
$node = Pop(nodeQueue)$
if $(\ nodedataSize \geq minSplitTreshold)$: // check if the current node need split or not
$K = FeatureChosen(F)$ // generating split feature subsets from *F dimension land-use features*
$bestSplitValue = MinSplitVariance(K)$ // filtering the best split value
$SplitDataSample(node, bestSplitValue)$// partitioning the node data samples
$leftNode = MakeNode(nodedataSample < bestSplitValue)$
$rightNode = MakeNode(nodedataSample \geq bestSplitValue)$
$nodeQueueInsert(leftNode, rightNode)$ // add the child nodes into the queue
else if
$node \rightarrow leafNode$ // nodes stop splitting and generating the leaf node
$leafNodeValue = Mean(nodedataSample)$
end if
end while
$lUCMappend(rootNode_i)$// add the newly generated decision into the forests
end for
return *LUCM*// output the constructed classification model

4. Classification Results and Accuracy

Based on Gee, the random forest algorithm was used to train the sample set by setting the number of decision trees to 500. The land-use information of the study area from 2009 to 2020 was extracted, and nine periods of land-use data were obtained. The classification results are shown in Figures 3 and 4.

In GEE, the classification results of each remote sensing image and sample points are analyzed for the accuracy of the confusion matrix, and the learning accuracy is calculated to verify the classification effect of the random forest algorithm. Overall accuracy (OA) and Kappa coefficient of classification results are calculated based on the confusion matrix to evaluate the reliability of classification results. The accuracy of classification results is shown in Table 3. The results show that the average overall classification accuracy is 89%, the Kappa coefficient is 88%, and the classification accuracy is high.

Table 3. Precision of the land-use classification results.

Land Type	2009	2010	2012	2014	2015	2016	2017	2019	2020
Water	96%	96%	94%	96%	91%	95%	92%	92%	94%
Construction land	86%	86%	84%	87%	83%	85%	83%	84%	85%
Forest	89%	91%	87%	90%	85%	88%	87%	86%	87%
Cultivated land	91%	90%	88%	92%	85%	89%	88%	87%	90%
OA	91%	91%	88%	91%	86%	89%	88%	87%	89%
Kappa	87%	86%	84%	88%	85%	86%	84%	83%	88%

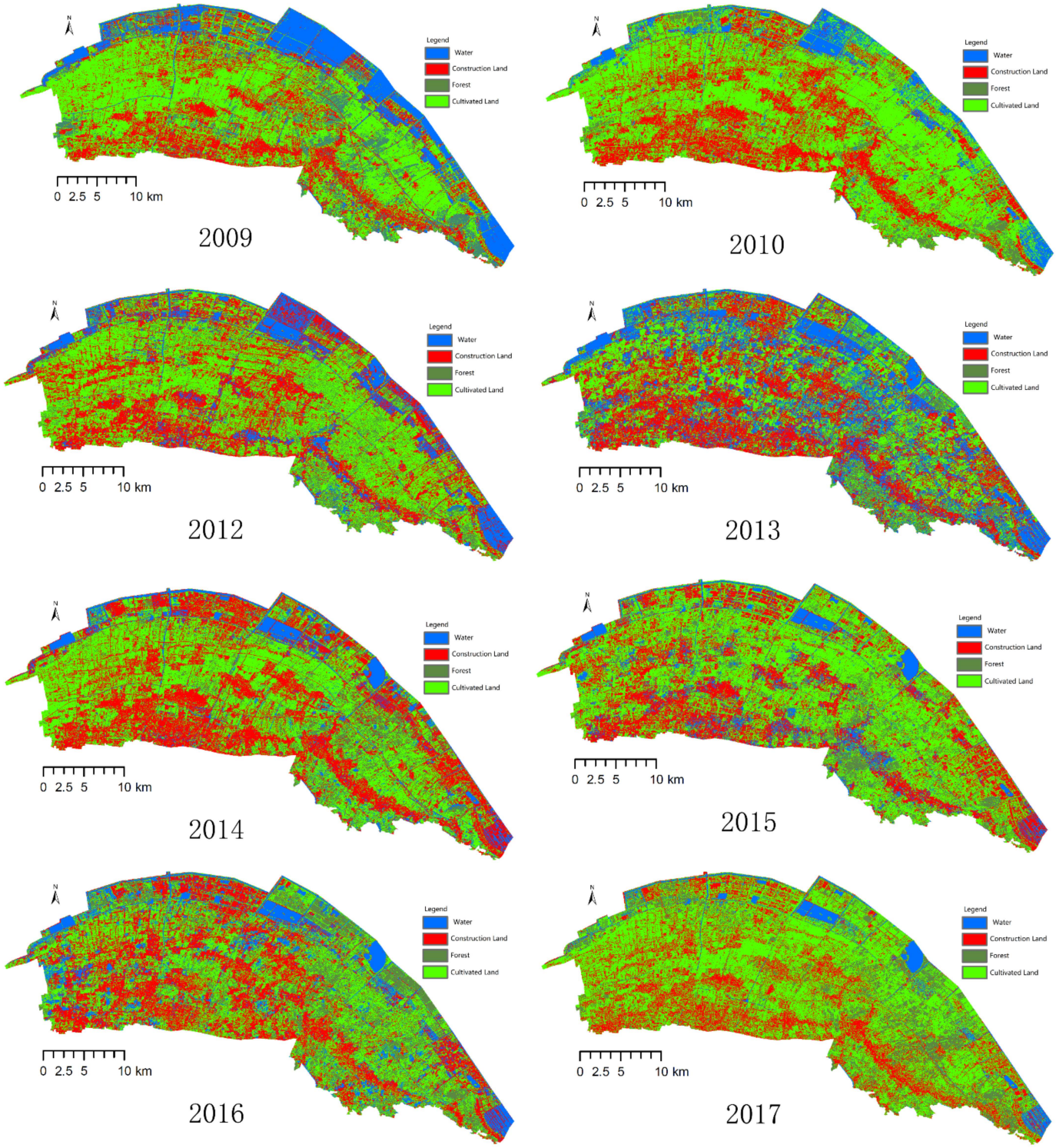

Figure 3. The land-use/land-cover contribution of the research area. (2009 to 2017).

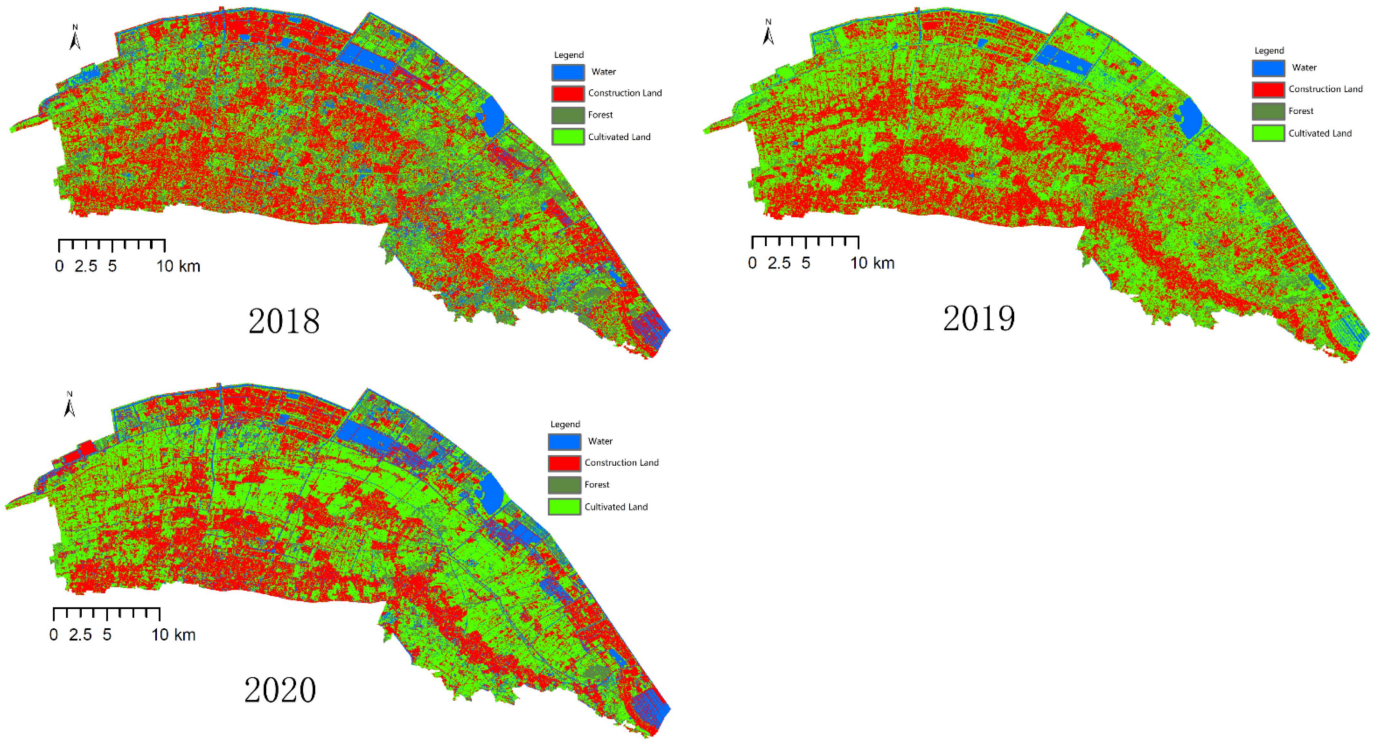

Figure 4. The land-use/land-cover contribution of the research area (2018 to 2020).

It can be seen from Table 3 that the maximum value of the overall classification accuracy and Kappa coefficient appeared in 2014, and the minimum value appeared in 2010 and 2015, which is related to the imaging quality of remote sensing images. The standard deviation of OA and Kappa coefficient is 1.77% and 1.22%, respectively, indicating that the accuracy of classification results in different periods is relatively stable. From the classification accuracy of various ground objects, the classification accuracy of water, cultivated land, and forest land is higher, while the classification accuracy of construction land is lower. The main reason is that the newly reclaimed land in the northern part of the study area is shown as a water body when it is flooded, while the surface reflectivity is high when it is exposed, which is easy to be mistaken for construction land. In addition, residential areas in some villages and towns are scattered, and mixed pixels are formed on remote sensing images, which are easy to be confused with cultivated land or forest land, resulting in missing or wrong points.

5. Analysis of the Temporal and Spatial Characteristics of LULC Change

5.1. Change of Land-Use/Land-Cover Distribution

Based on the interpretation of Landsat ETM +/oli data, nine land-use data were obtained from 2009 to 2020. The most intuitive performance of land-use change is the change of different types of land-use areas. By analyzing the change of each type of area, the trend of land use in this region can be understood. Table 4 shows the statistical results of various land-use types in the study area. The land-use pattern of the study area has changed greatly from 2009 to 2020. This is mainly reflected in the rapid growth of construction land, the decrease in the water body and woodland area in fluctuation, while the total amount of cultivated land remains stable.

Table 4. Land-use change from 2009 to 2020.

Year	Land-Use Type							
	Water		Construction Land		Forest		Cultivated Land	
	Area (km^2)	Proportion (%)	Area (km^2)	Proportion (%)	Area (km^2)	Proportion (%)	Area (km^2)	Proportion (%)
2009	128.6	14.7%	214.4	24.5%	110.0	12.6%	420.9	48.2%
2010	73.8	8.4%	246.0	28.2%	52.5	6.0%	501.7	57.4%
2012	116.8	13.4%	279.8	32.0%	75.6	8.7%	401.8	46.0%
2014	82.7	9.5%	315.5	36.1%	90.6	10.4%	385.1	44.1%
2015	97.2	11.1%	256.6	29.4%	83.9	9.6%	436.3	49.9%
2016	130.1	14.9%	282.8	32.4%	127.5	14.6%	333.5	38.2%
2017	40.6	4.6%	229.5	26.3%	116.5	13.3%	487.4	55.8%
2019	34.4	3.9%	326.6	37.4%	59.6	6.8%	453.4	51.9%
2020	107.2	12.3%	315.0	36.0%	39.9	4.6%	411.8	47.1%

The area ratio of various land-use types in the study area from 2009 to 2020 is shown in Figure 5, and the change trend is shown in Figure 6. The results show that from 2009 to 2020, the land-use distribution in the study area is relatively stable. Cultivated land accounts for about 50% of all land-use types, which is the largest and most widely distributed land-use factor type. During the whole study period, the area of forest land and water body generally decreased, and the building land showed a sharp expansion. The growth of economic construction, the increase in population pressure, the expansion of cities and towns, and the vigorous development of tourism all lead to the increasing demand for construction land and the expanding area of construction land. The decrease in water area is mainly due to the rapid economic development along the river, which results in the squeezing of water area. This has negative effects on ecological environment protection, flood drainage, and farmland irrigation in the study area.

In this paper, to analyze the changes more accurately in the land-use distribution in the study area, information entropy, equilibrium, and dominance are used to evaluate the changes in land-use distribution. The calculation results of land-use information entropy, equilibrium degree, and dominance degree are shown in Table 5, and the changes are shown in Figure 7.

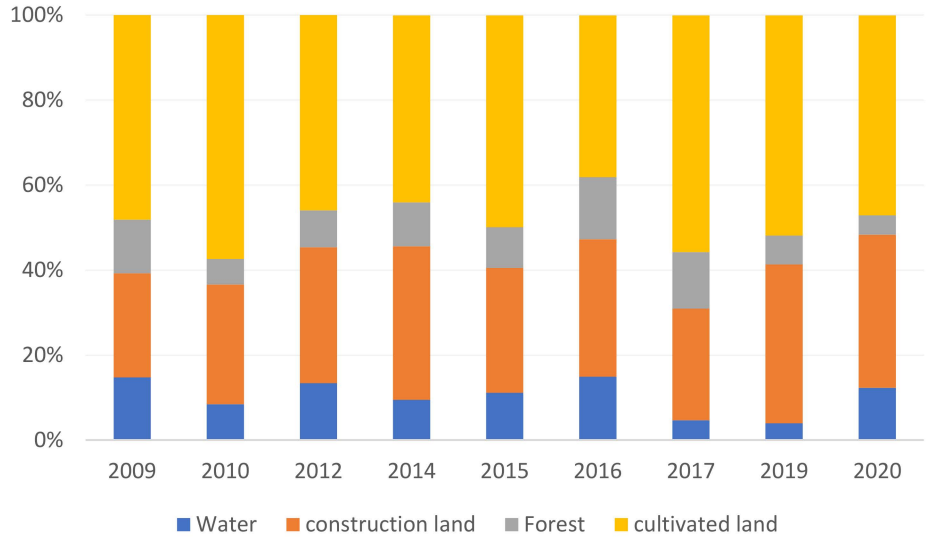

Figure 5. The area and proportion of various land-use types in the research area.

Figure 6. The change trend of land-use type area during 2009-2020.

Table 5. Information entropy, dominance, and equilibrium degree of land use.

	2009	2010	2012	2014	2015	2016	2017	2019	2020
Entropy	1.24	1.05	1.20	1.19	1.18	1.30	1.09	1.02	1.12
Equilibrium degree	0.89	0.76	0.87	0.86	0.85	0.94	0.78	0.73	0.81
degree of domination	0.11	0.24	0.13	0.14	0.15	0.06	0.22	0.27	0.19

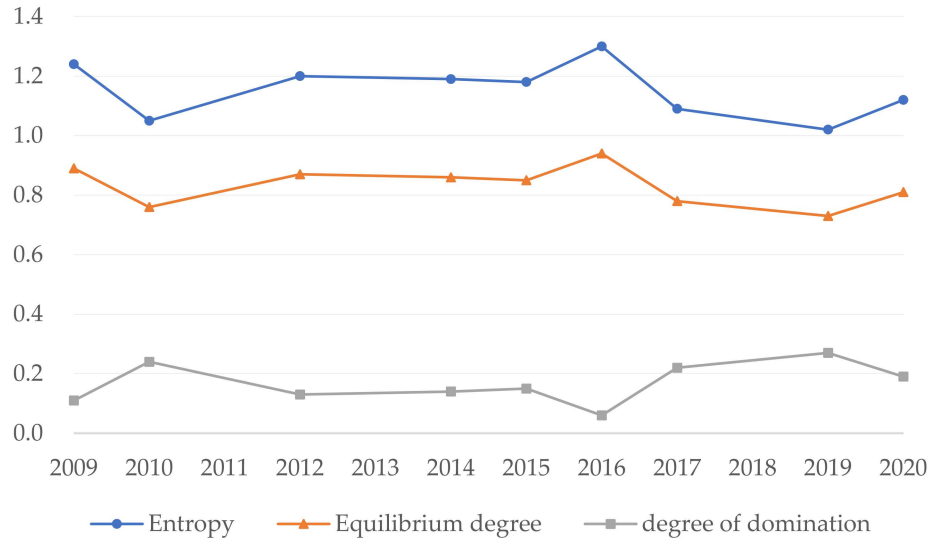

Figure 7. The change of information entropy, equilibrium degree, and dominance degree of land use.

The land-use system in the study area is very complex, which is influenced by the natural environment, social policy, economy, and human factors. The information entropy fluctuates at a high level with an average value of 1.15; however, the multi-year average of the equilibrium degree is as high as 0.83, and the land-use distribution has strong equilibrium and high complexity. The dominant land class has a low degree of domination over this region.

The intensity of human activities has a great impact on the structure of regional land use. The regional development mode, economic development level, industrial structure

and ecological environment construction are all closely related to the regional land resource system, which causes the change of land-use information entropy. The land-use system in the coastal plain has low stability and high complexity. From the change of information entropy, the anti-interference ability of the land-use system is relatively poor, and the stability of the land-use system in the process of regional development is relatively low. At the same time, the equilibrium degree of land use is relatively high, which means an obvious fluctuation, indicating that the structure of the land-use system is relatively balanced and land-use conversion is relatively frequent. The dominance of land-use showed a small upward trend, indicating that the dominance of land-use types as dominant resources increased, while the dominance of other land types decreased.

The calculation results of patch density in the study area are shown in Figure 8. The patch density is between 70 pieces/km^2 and 110 pieces/km^2, showing a relatively broken state. The patch density in the study area increased continuously from 2009 to 2016, decreased rapidly from 2016 to 2019, and increased again in 2020. The results showed that the fragmentation degree of land use increased first, then decreased, and then increased.

The calculation results of the fragmentation degree of each land-use type in the study area are shown in Figure 9. The land-use types in the study area are highly fragmented and change obviously year by year. Among them, the fragmentation degree of cultivated land is the lowest, and the number of patches per square kilometer is maintained at about 50, among which it will return after reaching the maximum peak in 2016, and the overall fragmentation degree will increase slightly with time. The degree of forest land fragmentation is the highest, and it fluctuates greatly with time. Since 2009, water fragmentation has been increasing continuously, reaching 247 patches per square kilometer in 2015, then decreasing rapidly in the next two years, and increasing again from 2017 to 2020. Contrary to water and cultivated land, the fragmentation degree of construction land showed a trend of first decreasing, then increasing and then decreasing, reaching the maximum value in 2017, and then gradually decreasing.

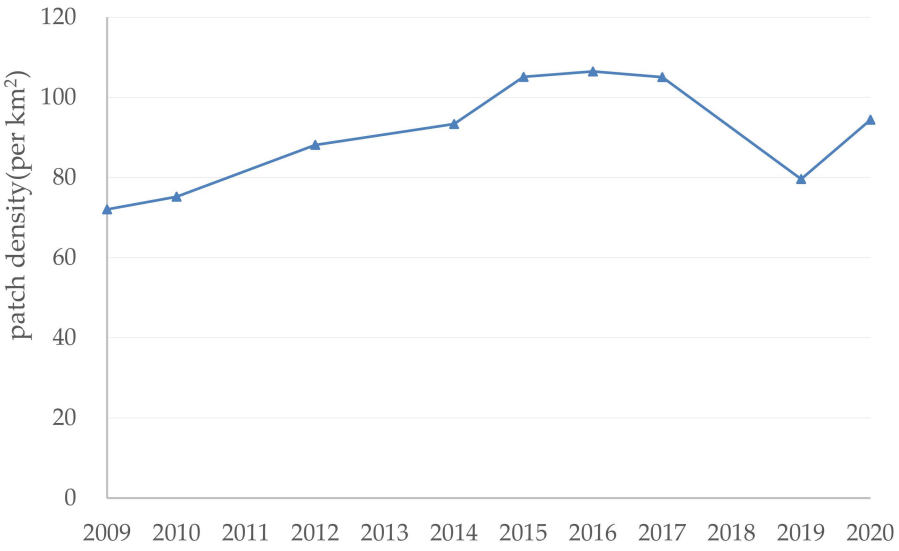

Figure 8. Changes of patch density in the research area.

By comparison, it was found that the fragmentation degree of water and cultivated land was close in 2009. It gradually increased, and then decreased after reaching the maximum in 2015 and 2016. Finally, it began to increase again after 2017. The fragmentation degree of construction land showed the opposite trend, which was higher at the initial stage of the study, and then decreased, and rebounded slightly after reaching the minimum in 2014. The fragmentation degree was still low in 2016 and increased in 2017.

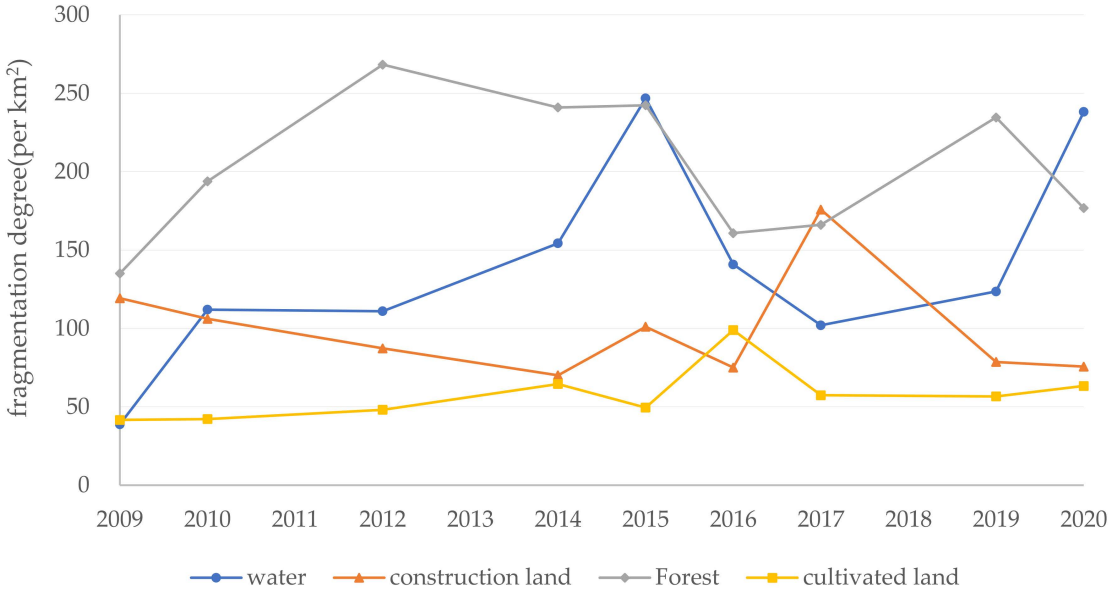

Figure 9. Fragmentation of different types of land use.

5.2. Change of Land-Use/Land-Cover Intensity

As a kind of natural complex, under the influence of human activities, the original natural attributes of land are decreasing, and different land-use types represent the characteristics of land-use intensity to a certain extent. According to the research results of relevant scholars and the characteristics of land use in the study area, this paper divides the land into three grades according to the maintenance status of social influence factors, and the selected grading index is shown in Table 6.

Table 6. Land-use degree.

Land-Use Degree	City and Town Settlement Land	Agricultural Land	Forest, Grass, and Water Land
Land-use type	Construction land	Cultivated land	Forests and Water
Classification Level	4	3	2

The comprehensive index of land-use intensity in each target year is calculated, and the results are shown in Table 7. The change of land-use intensity is shown in Figure 10.

It can be seen from Table 6 and Figure 10 that, considering the change range of land-use intensity index (100–400), the development degree of land resources in the study area is relatively high during the whole study period, and the land-use intensity index generally shows an upward trend in fluctuation. The negative growth of land-use intensity in 2014–2016 was mainly due to the influence of policy factors related to the balance of cultivated land occupation and compensation, such as "Notice of the General Office of Zhejiang Provincial People's Government on Further Strengthening the Management of Balance of Cultivated Land Occupation and Compensation". The growth trend of construction land in the study area was restrained during this period, while the cultivated land area remained basically stable, making the overall land development and utilization intensity weakened and declined.

Table 7. The index of land-use intensity in the research area.

Year	2009	2010	2012	2014	2015	2016	2017	2019	2020
Land-use level index	297.2	313.7	310.0	316.2	308.6	302.9	308.3	326.6	319.2

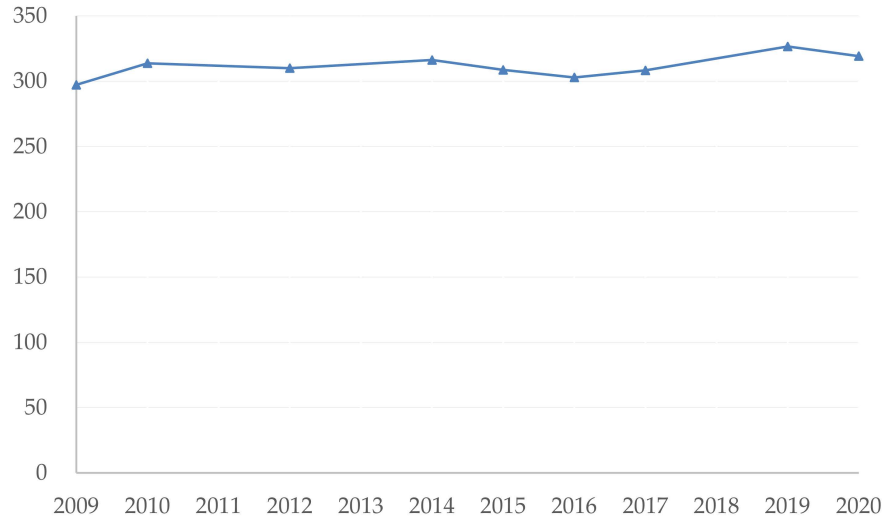

Figure 10. The change of land-use intensity index.

To analyze the influence of the change of land-use intensity on the structure and pattern of land use in the basin, based on the previous analysis, a scatter diagram of land-use intensity and land-use distribution index was made. As shown in Figure 11, land-use intensity has an obvious influence on the pattern. Land-use intensity is negatively correlated with information entropy value and equilibrium degree, and positively correlated with dominance degree; however, there is no obvious correlation between land-use intensity and patch density and fragmentation.

In areas where human activities are dominant, land-use intensity can accurately reflect the breadth and depth of land use and the interference intensity of human activities on the land ecosystem. The study area is in the northern plain of Cixi City. For a long historical period, there have been obvious traces of reclamation and development of tidal flats on a large scale. With the increasing intensity of land development and utilization, the land-use distribution of the basin has changed obviously. The decrease in information entropy and balance means that the diversity of land use is reduced, the land-use types are more intensive, and individual landscape types gradually occupy a dominant position.

5.3. Direction of Land-Use/Land-Cover Change

To detect the land-use change of each land type in the study area from 2009 to 2020, remote sensing change detection theory is used to analyze the spatial change characteristics of land use in this study. Pattern recognition and change information extraction were carried out by using the earth observation data of two phases, to quantitatively analyze and determine the characteristics and process of ground object change. Change detection involves the number and distribution of changes. For images in different periods in the same area, it is necessary to calculate the types, boundaries, and trends of objects before and after changes, and then analyze the characteristics and reasons for these dynamic changes.

In this paper, the image change information of the study area from 2009 to 2020 was extracted based on GEE, and the information was classified and compared. The thematic classification maps of remote sensing images in front and back phases were used for overlay analysis, to judge the classification attribute of each pixel in the thematic maps of front and back phases and count its change information. The method directly obtains the type, quantity, and position of changes and avoids the data mismatch caused by different sensors or different acquisition seasons. It can also avoid the influence of time phase difference and radiation correction on change detection results.

The detection results of land-use change in the study area from 2009 to 2020 showed that the area of cultivated land, construction land, forest land, and water body accounted for 47.3%, 36.3%, 4.4%, and 11.9%, respectively, in 2020. The land-use transfer matrix is shown in Table 8.

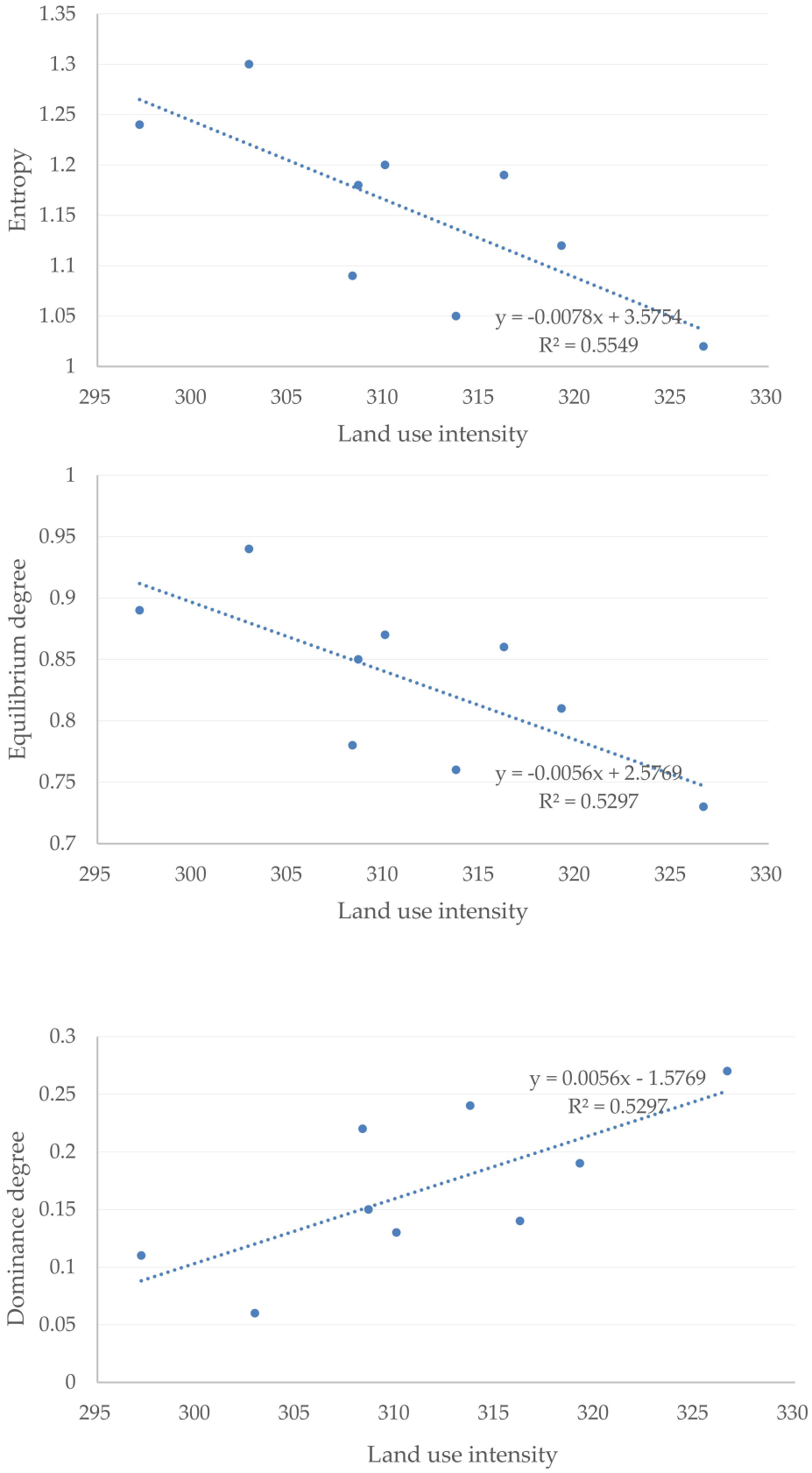

Figure 11. Fitting of the correlation between land-use intensity and entropy, equilibrium degree, and dominance degree.

Table 8. Regional land-use transformation matrix from 2009 to 2020 (area unit: km^2).

Before Transformation	After Transformation					Total Area in Year 2009
	Transformation Area and Ratio	Cultivated Land	Construction Land	Forest	Water	
Cultivated land	Area	261.6	129.5	8.4	20.3	419.8
	Out-transformation ratio	62.30%	30.90%	2.00%	4.80%	
	In-transformation ratio	64.10%	41.30%	21.90%	19.70%	
Construction land	Area	62.8	122.9	3.3	19.7	208.7
	Out-transformation ratio	30.10%	58.90%	1.60%	9.50%	
	In-transformation ratio	15.40%	39.20%	8.60%	19.20%	
Forest	Area	59.3	23.9	15.7	8	106.9
	Out-transformation ratio	55.50%	22.30%	14.70%	7.50%	
	In-transformation ratio	14.50%	7.60%	41.00%	7.80%	
Water	Area	24.2	37.3	11	54.9	127.3
	Out-transformation ratio	19.00%	29.30%	8.60%	43.10%	
	In-transformation ratio	5.90%	11.90%	28.50%	53.30%	
Total Area in year 2020		407.9	313.5	38.4	102.9	862.7

All kinds of land-use transfers in the region are obvious. In recent 12 years, the area where the land-use type has not changed accounts for 52.7%, and the mutual conversion area between cultivated land and construction land is relatively large. The changed land types are as follows: cultivated land decreased by 2.8%, construction land increased by 50.2%, forest land decreased by 64.1%, and water bodies decreased by 19.2%.

In the cultivated land area in 2020, the proportions of construction land transfer, forest land transfer, and water area transfer were 15.4%, 14.5%, and 5.9%, respectively. In the construction land area, the proportions of farmland transfer, forest land transfer, and water area transfer were 41.3%, 7.6%, and 11.9%, respectively. The forest land area decreased by 68.5 km^2 in 12 years, only 15.7 km^2 of the original forest land area remained, and the cultivated land, construction land, and water body accounted for 21.9%, 8.6%, and 28.5%, respectively. There were transformations between water body and cultivated land, construction land, and forest land. The existing water body area was 20.3 km^2 from cultivated land, 19.7 km^2 from construction land, and 8 km^2 from forest land, accounting for 19.7%, 19.2%, and 7.8%, respectively. The area of water body transferring into corresponding land-use types was 24.2 km^2 of cultivated land and 37.3 km^2 of construction land was 11.0 km^2, the proportion of water to construction land is the largest, and the transfer-out rate is 29.3%.

Due to the rapid economic growth, the continuous adjustment of industrial structure in the region, the vigorous development of industry, agriculture, and tourism, the aggregation and flow of population, and other reasons, the four types of land use have a mutual conversion, generally showing the trend of farmland, woodland, water transfer to construction land, and woodland transfer to cultivated land.

Under the background of urbanization, many cultivated lands are occupied by urban expansion. At the same time, to make up for the loss of these cultivated land, according to the policy of "balance of occupation and compensation", newly cultivated land should be added in the areas with a short reclamation period, and the index of urban construction

land should be exchanged in proportion; therefore, the total amount of land in this region remains unchanged but shows frequent mutual conversion among various land-use types.

Cultivated land, construction land, forest land, and water all have a mutual transformation, but the total area remains basically stable in the fluctuation. Due to a large number of small rivers, ditches and ponds, and fishery ponds in the region, there is a mutual conversion between the water area and cultivated land, forest land and construction land, and the water area has had a downward trend in the past 12 years. The same phenomenon that occurred for the water body area also occurred in woodland, but the downward trend of woodland was more obvious, from 106.9 km^2 to 38.4 km^2. The total increase in land-use type is only construction land, and the area increased by 104.8 km^2, an increase of 50.2%.

5.4. Land-Use/Land-Cover Change Rate

To compare the differences and changing trends of different land-use types, this study quotes the dynamic attitude of land use to quantitatively reflect the changing rate of land-use types through the dynamic attitude of a single land-use type.

The calculation results of the annual change rate of four land-use types in the study area are shown in Table 9; the land-use transformation matrix is listed in Table 10. The results show that the overall dynamic change of land use was not significant from 2009 to 2020, and the land-use attitude of forest land and construction land was −5.31% and 3.91%, respectively, and the cultivated land and water body decreased slightly; however, the calculated data year by year show that the land use in the study area has changed rapidly in the past 12 years, in which water, construction land, cultivated land, and forest land have increased or decreased in different degrees in each year. The dynamic attitude of land use shows that the land-use category changes strongly, and the stability is poor.

Table 9. Land-use dynamic index in research area.

Period	Water	Construction Land	Forest	Cultivated Land
2009–2010	−21.31%	7.38%	−26.15%	9.59%
2010–2012	19.40%	4.57%	14.71%	−6.63%
2012–2014	−9.72%	4.26%	6.61%	−1.39%
2014–2015	8.74%	−9.34%	−3.72%	6.65%
2015–2016	16.95%	5.11%	26.02%	−11.78%
2016–2017	−34.38%	−9.43%	−4.33%	23.07%
2017–2019	−5.14%	14.11%	−16.27%	−2.32%
2019–2020	106.01%	−1.77%	−16.51%	−4.59%
2009–2020	−1.39%	3.91%	−5.31%	−0.18%

Table 10. Land-use transition matrix of the research area.

Land Type	Cultivated Land	Construction Land	Forest	Water	Total Area in 2009
		Period 2009 to 2010			
Cultivated land	310.71	94.56	9.97	4.71	419.96
Construction land	75.40	125.00	4.99	3.51	208.89
Forest	64.41	11.46	28.86	2.35	107.08
Water	50.51	9.01	5.94	62.05	127.51
Total area in 2010	501.03	240.03	49.76	72.62	863.44

Table 10. *Cont.*

Land Type	Cultivated Land	Construction Land	Forest	Water	Total Area in 2010
		Period 2010 to 2012			
Cultivated land	292.58	123.71	46.70	38.01	501.01
Construction land	80.23	130.36	5.86	23.56	240.01
Forest	24.44	5.02	15.74	4.55	49.75
Water	6.39	16.37	1.38	48.46	72.61
Total area in 2012	403.65	275.46	69.68	114.58	863.37
Land Type	Cultivated Land	Construction Land	Forest	Water	Total Area in 2012
		Period 2012 to 2014			
Cultivated land	240.46	97.24	49.37	16.44	403.52
Construction land	86.06	160.10	15.92	13.15	275.23
Forest	42.20	8.26	14.30	4.83	69.59
Water	13.53	50.08	5.57	45.16	114.33
Total area in 2014	382.26	315.67	85.15	79.59	862.67
Land Type	Cultivated Land	Construction Land	Forest	Water	Total Area in 2014
		Period 2014 to 2015			
Cultivated land	260.08	63.26	43.52	15.37	382.22
Construction land	98.07	165.59	13.64	38.32	315.62
Forest	56.71	13.25	13.51	1.67	85.14
Water	22.87	11.08	8.13	37.48	79.57
Total area in 2015	437.74	253.17	78.79	92.85	862.55
Land Type	Cultivated Land	Construction Land	Forest	Water	Total Area in 2015
		Period 2015 to 2016			
Cultivated land	210.99	104.60	78.70	43.48	437.77
Construction land	67.06	139.22	9.39	37.51	253.19
Forest	31.13	10.76	32.14	4.79	78.81
Water	20.81	28.13	3.11	40.86	92.90
Total area in 2016	329.99	282.70	123.34	126.64	862.67
Land Type	Cultivated Land	Construction Land	Forest	Water	Total Area in 2016
		Period 2016 to 2017			
Cultivated land	222.48	60.66	46.11	0.75	330.00
Construction land	148.49	127.79	5.18	1.24	282.71
Forest	62.07	8.10	53.09	0.10	123.35
Water	54.83	25.08	8.75	38.01	126.66
Total area in 2017	487.86	221.63	113.14	40.09	862.72

Table 10. *Cont.*

Land Type	Cultivated Land	Construction Land Period 2017 to 2019	Forest	Water	Total Area in 2017
Cultivated land	299.18	163.22	23.03	2.42	487.85
Construction land	69.64	146.86	4.15	0.97	221.62
Forest	72.26	11.34	28.72	0.80	113.13
Water	10.58	0.71	0.04	28.76	40.09
Total area in 2019	451.67	322.13	55.94	32.95	862.69
Land type	**Cultivated Land**	**Construction Land Period 2019 to 2020**	**Forest**	**Water**	**Total Area in 2019**
Cultivated land	272.91	106.41	20.95	51.40	451.66
Construction land	103.83	200.63	1.47	16.20	322.12
Forest	30.26	5.18	15.95	4.54	55.94
Water	0.88	1.27	0.02	30.77	32.94
Total area in 2020	407.88	313.49	38.39	102.91	862.67

According to the land-use transfer matrix, the change lines of land-use transfer in and out were drawn. According to the land-use transfer matrix, we draw the change line of land use in and out of the study area. Figure 12 shows the destination of cultivated land reduction and the source of expansion in the most recent 12 years. The results showed that 38% of cultivated land was transferred to other land types on average every year, which was mainly converted into construction land. The construction land occupied 102 km^2 of cultivated land on average every year, accounting for 24% of cultivated land area and 62% of the total transferred area. In addition, 40 km^2 of cultivated land is converted into forest land and 22 km^2 into water bodies every year. Cultivated land has been invaded and expanded outward, with an average of 91 km^2 of construction land being restored to cultivated land every year, accounting for 21% of the cultivated land area. In addition, many forest land and water bodies are reclaimed as cultivated land every year, accounting for 11% and 5% of the cultivated land area, respectively.

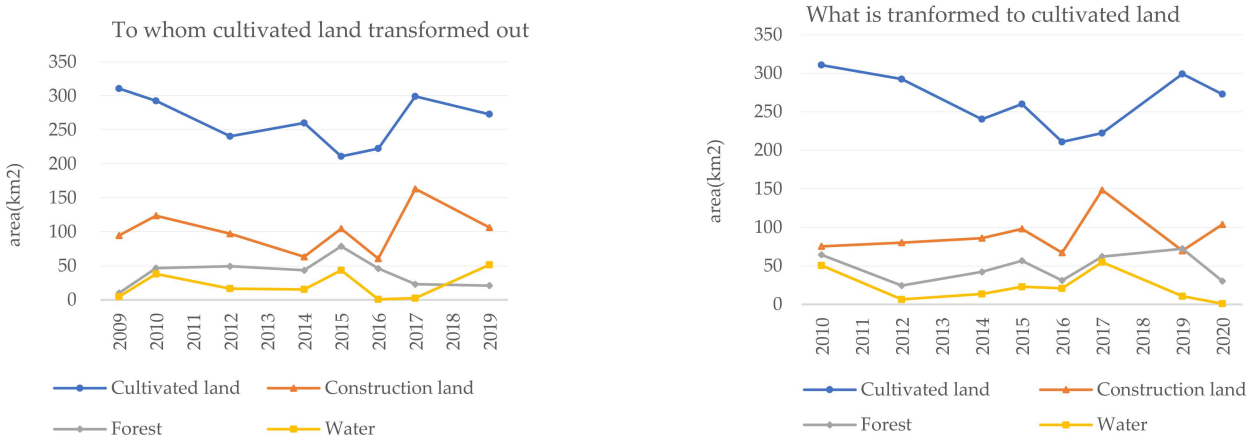

Figure 12. Changes of cultivated land in the studied area.

Figure 13 shows the destination of construction land and the source of expansion in the most recent 12 years. The results show that the construction land is transferred

out frequently, with an average of 44% of the area transferred out into other land types every year, mainly into cultivated land, and the area converted from construction land into cultivated land accounts for 79% of the total transferred-out area, which makes up for the occupation of cultivated land to a great extent and keeps the cultivated land area basically balanced. In addition, an average of 7.6 km^2 of construction land is converted into forest land and 17 km^2 into water bodies every year. When the construction land expands outward, it will also occupy forest land and water, accounting for 3% and 6% of the construction land area, respectively.

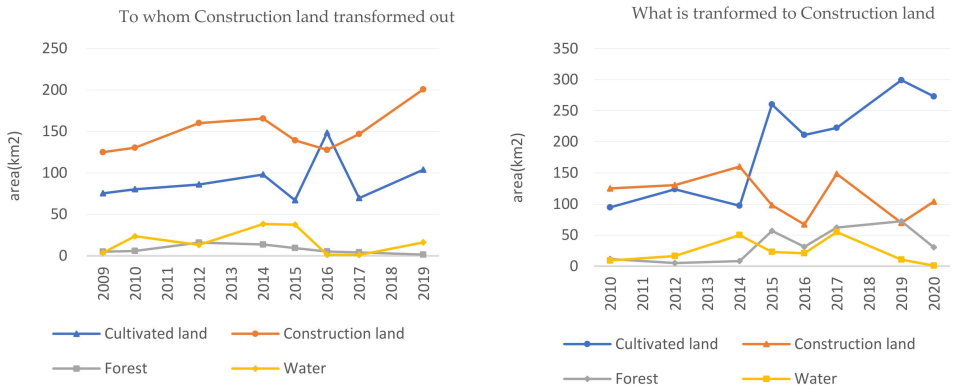

Figure 13. Changes of construction land in the studied area.

Figure 14 shows the change of forest land. Cultivated land is the main source of forest land transfer and expansion. On average, 56% of forest land is converted into cultivated land every year, and 52% of forest land is transferred from cultivated land every year. It can be seen from Figure 14 that the peak time difference between forest land and cultivated land is no more than two years, and the dynamic balance is maintained during the change.

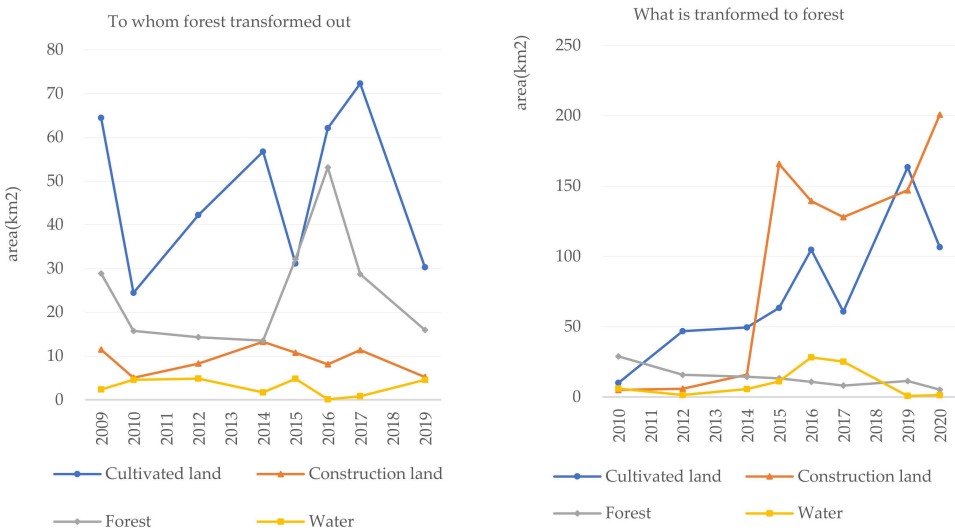

Figure 14. Changes of forest land in the studied area.

Figure 15 shows the change of the water body area. The results show that 52% of the water area is transferred to other land types on average every year, mainly into cultivated land and construction land. Cultivated land and construction land occupy 22.6 km^2 and 17.7 km^2, respectively, on average every year, accounting for 47% of the water area and 91% of the total transferred water area. In addition, an average of 21.6 km^2 of cultivated land and 16.8 km^2 of construction land are converted into water bodies every year. The balance between occupation and compensation was basically maintained.

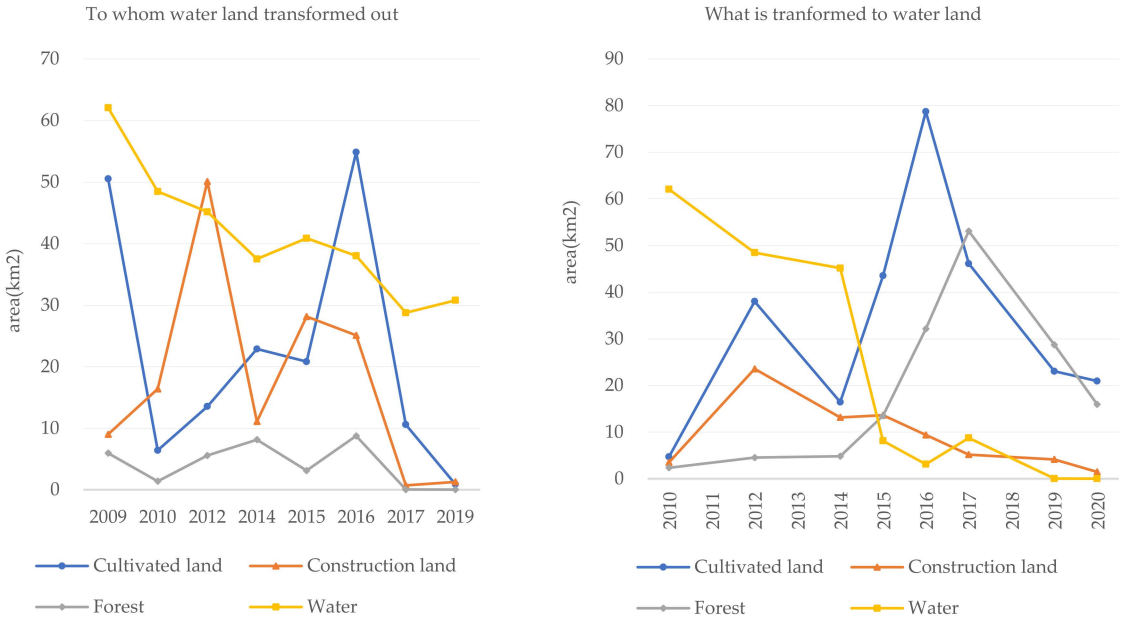

Figure 15. Changes of water land area in the studied area.

5.5. The Driving Force of Land-Use/Land-Cover Change

The driving forces of land-use transition and its magnitude depended on the type of land use. To determine the driving forces of land-use change in the study area, quantitative and qualitative analyses were applied. To assist the driving force analysis, we collected relevant social-economic data, including population, economy, and environmental survey statistics [18–23].

Since 2009, the land use in the study area has undergone dramatic changes. The impacts of urbanization, the balance of cultivated land occupation and compensation, and the construction of economic development zones are all reflected in the land-use changes in the study area.

(1) From 2009 to 2020, the land-use distribution in the study area was relatively stable. Among various land-use types, cultivated land accounted for about 50%, which was the largest and most widely distributed land-use factor type. During the whole study period, the area of forest land and water body generally decreased, and the building land showed a sharp expansion trend.

(2) The land-use system in the study area is very complex, which is affected by the natural environment, social policy, economic and cultural factors, and the information entropy fluctuates at a high level with an average value of 1.15. The multi-year average of equilibrium degree is as high as 0.83. The balance and complexity of land-use distribution are strong, and the dominance of dominant land types in the region is low. In the process of regional development, the stability of the land-use system is low, and the anti-interference ability is relatively poor. At the same time, the structure of the land-use system is relatively balanced, and land-use conversion is relatively frequent.

(3) The landscape patch density in the study area showed a trend of first increasing, then decreasing and then increasing, and the overall land use was relatively fragmented. Among them, arable land has the lowest degree of fragmentation. After reaching the maximum peak in 2016, the overall degree of fragmentation increased slightly. Woodland has the highest degree of fragmentation and fluctuates greatly over time. The water fragmentation first increased, then decreased and then increased, and the construction land showed the opposite trend.

(4) The trace of beach reclamation and development in the study area is obvious, the degree of land resources development is high, and the intensity of land-use rises

in fluctuation. With the increasing intensity of land development and utilization, the land-use distribution in the basin has changed obviously. Land-use diversity decreases, land-use types become more intensive, and individual landscape types gradually occupy a dominant position.

(5) The total amount of regional land remains unchanged, but there are frequent mutual conversions among various land types. The area where land-use types have not changed in the past 12 years only accounts for 52.7%. The main types of land that have changed are listed as follows: arable land has decreased by 2.8%, construction land has increased by 50.2%, forest land has decreased by 64.1%, and water bodies have decreased by 19.2%.

(6) From 2009 to 2020, the overall dynamics of land use have not changed much, but year-by-year calculation data show that the land-use change rate in the study area has been rapid in the past 12 years. On average, 38% of the cultivated land is transferred out to other land types each year, of which 62% is converted to construction land. At the same time, an average of 44% of the construction land is transferred to other land types each year, of which 79% is converted to cultivated land. The main sources of transfer and expansion of forest land and water bodies are cultivated land and construction land, and each land type maintains a dynamic balance of occupancy and compensation as it fluctuates and grows.

The change of land-use function directly reflects the influence and disturbance of the development of human social and economic activities on the evolution of the terrestrial ecosystem of the Earth. At the same time, land use is also a bridge connecting human beings with the natural ecological environment in their production activities. Changes in land-use function can characterize the energy circulation and material flow between the Earth's atmosphere, soil, biosphere, lithosphere, and hydrosphere.

We chose the nine parameters to build our driving force model for the research area, integrating the factors from different dimensions, such as population, economic development, agriculture, forest industry, construction industry, etc.

The driving force of the land-use change can be summarized as follows:

(1) Demographics and human population dynamics, including population growth and migration. The annual residential population of Cixi city grew from 1.86 million to 2.23 million, indicating a 19.9% population growth. Meanwhile, the urban population grew from 0.183 million to 0.744 million; the rural population decreased from 0.852 million to 0.318 million. The growth of the urban population also results in the transition from forest land and cultivated land to construction land, and the transition from forest land to cultivated land; therefore, the intensity of population and economic growth are the main driving forces of the land-use change in the study area.

(2) Economic development. The gross domestic product of the research area grew from 62.5 billion RMB to 200.8 billion RMB, representing a 2.21X growth from year 2009 to year 2020. The Cixi municipal government reorganized the industrial sector structure, coordinated and optimized the development of agriculture, industry, and service sectors, which ultimately increased the gross domestic products of Cixi city significantly. Although the gross product of the agriculture sector of the research area increased dramatically from the year 2009 to the year 2020, the agricultural contribution in the economy of Cixi city decreased due to the human population transition from agriculture to the industry sector. Moreover, the increase in the industry sector demands more and more construction lands from other sectors.

(3) Urbanization. In the last two decades, China has been undergoing unprecedented economic growth, massive rural-to-urban migration, and large-scale policy-driven ecological restoration. Eastern China is one of the most vibrant areas in terms of economic growth and human activities. The selected research area in this paper went through a fast urbanization process in the last 12 years, while large numbers of people become permanently concentrated in cities from rural areas. The city area expanded dramatically, and the construction lands occupied the agricultural and

forest land. Moreover, the urbanization process also demands more land to provide public infrastructures such as roads and residential regions, which also made an important impact on land-use change. Urbanization, as an important socioeconomic factor, plays a vital role in promoting land-use transition. Although the interaction relationship between urbanization and land-use transition, from the perspective of population urbanization, economic urbanization, and social urbanization, is complex, the level of land-use morphologies from the perspective of dominant and recessive morphologies of land-use is a meaningful and good indicator for environmental evaluation. From our analysis, the relationship between urbanization and the land-use transition is not a simple linear relationship but tends to be complex with the process of urbanization, and reasonable urbanization and land-use morphologies will promote further benign coupling in the system.

(4) The coupling effects of all kinds of human activities. Natural population transition, economic growth, and industry sector change are typical human activities, and we cannot separate one dimension from another to account for the driving force of land-use change in the target area. Specifically, the land-use change of one region is affected by the coupling effects of such kinds of human activities.

The driving force of land-use/land-cover change varied greatly with space, time, and land-use type. For example, socioeconomic development was the main driving force for the built area expansion, and geographical differentiation was the dominant factor in the conversion of cultivated land, forest land, and grassland. The driving forces of land-use types presented in this paper can help develop strategies for sustainable development in coastal plains in China and may also pose as a reference in other countries or regions. These findings would provide decision support for policymakers to formulate future sustainable land-use policies.

6. Related Work

Human beings cannot live without well-managed, multi-functional lands. Land is usually defined as a physical entity in terms of its geography and spatial nature, which contains natural resources such as soil, minerals, water, and biota. These components on the land provide a variety of essentials to the maintenance of life-support systems and the productive capacity of the environment. Land is the terrestrial foundation of society, and it is the platform for infrastructure and for residential, commercial, and industrial areas, and is a source of economic growth; however, with the increasing human activities, including industrialization, urbanization, and agriculturalization, the impact of land-use systems on global climate change has become increasingly significant and an increasing concern for both government and the nature. Moreover, the increasing share of the planet's land area is in some way modified by human activities, leading to unsustainable changes in our landscapes. Both macro and micro-level ecological evolution and interaction can have an impact on the land-use process [24]. At the same time, land use in specific areas changes due to the change of climate, human migration, and land transition. In some regions, climate change and severe weather events, such as floods and drought, stress land resources. In extreme cases, such changes might lead to unhealthy and degraded lands.

Machine learning techniques have provided excellent results in applications ranging from parameter estimation to image classification and anomaly detection. In recent years, machine-learning-based approaches were proposed to assist the land-use classification in multiple scale levels. Deep learning is used for the object-based classification of high-resolution remote sensing images to improve classification accuracy. For example, Zhang et al. [25] proposed joint deep learning (JDL) for land cover and land-use classification, which incorporated patch-based convolutional neural networks (CNNs) and pixel-based MLP with joint reinforcement and mutual complementarity; they used a Markov process through iterative updating for joint distributions between land cover and land use.

The conventional pixel-based land-cover classification methods label each pixel independently by considering only a pixel's spectral properties. These purely spectral-based

techniques may be applicable to many medium and coarse-scale remote sensing analyses. However, with the advances in sensor technologies, remote sensing images have higher resolution, which leads to the problem that, in some cases, the pixels are smaller than the objects to be classified. Zou et al. [26] proposed a spatialized classification approach for hyperspatial imagery, which uses pixels within a fixed window as predictors in a classifier and can classify different types of vegetation; however, this method is only designed for mapping vegetation growth forms such as trees, shrubs, and herbs in a forested ecosystem in the Sierra Nevada Mountains.

Marcos et al. [27] proposed a CNN architecture called Rotation Equivariant Vector Field Network (RotEqNet) to encode rotation equivariance in the network itself. They use rotating convolutions as building blocks and only pass the values corresponding to the maximally activating orientation throughout the CNN network in the form of orientation encoding vector fields. The proposed RotEqNet treats rotated versions of the same object with the same filter bank and therefore achieved state-of-the-art performances even when using very small architectures trained from scratch. The proposed approach can be used for land-cover mapping from sub-decimeter resolution remote images.

However, land-use classification is an inadequate process due to a lack of data, especially for undeveloped nations. Researchers combined data from multiple sources for land-use classification. Srivastava et al. [28] proposed a CNN model to predict land use at the object level from multi-modal data from aerial and ground views: overhead imagery from Google Maps and ensembles of ground-based pictures (side-views) per urban-object from Google Street View (GSV). They used an end-to-end trainable model, which uses OpenStreetMap annotations as labels. The model can accommodate a variable number of GSV pictures for the ground-based branch and can also function in the absence of ground pictures at prediction time. The proposed approach is only suitable for land-use map updates in cities, not for rural areas, forests, water, etc.

The complexity and heterogeneity of land-use characteristics lead to the gap between the inferable low-level image features and high-level semantic function representation [29,30]. Markov random field, object-based image analysis (OBIA), pixel-based CNN, object-based CNN, multiple-scale CNN, and joint deep learning were proposed for land-use classification. To improve the land-use classification accuracy of irregular segments output by segmentation methods according to the corresponding ground objects, Pan et al. [29] proposed a simplified object-based deep neural network (SO-DNN) for very-high-resolution remote sensing image classification, which uses a new segment category label inference method as the classification model instead of a traditional CNN.

The present literature concentrates on the concept, definition, and classification of land use for the collection of environment statistics; however, the data collection process suffered due to a lack of resources and non-availability of statistical concepts, definitions, and classification. To handle satellite image data and other Earth observation data, Google Earth Engine (GEE), a cloud computing platform, was jointly developed by Google, Carnegie Mellon University, and the US Geological Survey. The public data set of the platform stores the complete image data of Landsat, Sentinel, MODIS, and other Earth observation satellites, and also includes climate prediction, land cover, and other geographic, environmental, and socioeconomic data sets [31]. The main functions of GEE can be realized by calling API provided in JavaScript and Python. Users can write programs according to their needs to realize remote sensing data processing and geospatial analysis. They can also reorganize existing algorithms and write more complex analysis programs. Meanwhile, the algorithms in GEE are constantly updated and enhanced [32–34].

Compared with the traditional remote sensing data processing and geospatial analysis methods, GEE can easily access massive data sets and have the ability of large-scale spatial calculation and analysis, which greatly improves the efficiency of geospatial data calculation and analysis. Considering that the Google Earth Engine platform can carry out interactive analysis and corresponding visualization and can have both fast data

acquisition and efficient calculation and analysis, the research on land-use monitoring and spatial-temporal change analysis in the study area is based on the GEE platform [35–37].

Random forests is a machine learning algorithm, which is a classifier with multiple decision trees. Random forest classifier achieves the purpose of classifying data sets by constructing many unrelated random decision trees, and leading and aggregating the decision trees through a prediction model. Compared with the maximum likelihood method, single decision tree, and single-layer neural network algorithm, the random forest algorithm has higher accuracy in processing high-dimensional data [38]. The random forest classifier is more robust than a single decision tree, and compared with other advanced classifiers, such as support vector machine (SVM), the random forest algorithm is easier to apply [39,40]. The random forest algorithm establishes a decision tree by searching the random subspace of a given feature set and sets the optimal splitting node by minimizing the correlation between the decision trees [41]. The random forest classifier can quantitatively set the contribution rate of each variable to the classification output to evaluate the importance of each variable. At the same time, the onboard random forest algorithm evaluates the internal accuracy through OOB (out-of-bag) technology, which takes about one-third of the data as an independent classification accuracy evaluation data set to cross-verify the reliability and accuracy of the classifier. Based on the superior performance of random forest algorithm, the mapping and classification of land-use information based on the random forest algorithm have been gradually started at home and abroad [38,42]. In this paper, our proposed model uses a random forest algorithm to assist the land-use classification and the classification accuracy is higher than 85%.

Tidal flats (non-vegetated area), along with coastal vegetation area, constitute the coastal wetlands (intertidal zone) between high and low water lines, and play an important role in wildlife, biodiversity, and biogeochemical cycles; therefore, land-use classification and analysis are fundamental for environmental and water resources evaluation in coastal plain areas; however, accurate annual maps of coastal tidal flats over the last few decades are unavailable, and their spatio-temporal changes in China are unknown. Wang et al. [43] analyzed all the available Landsat TM/ETM+/OLI imagery (~44,528 images) using the Google Earth Engine (GEE) cloud computing platform and proposed a decision tree algorithm to generate annual frequency maps of open surface water body and vegetation to produce annual maps of coastal tidal flats in eastern China from 1986 to 2016 at 30 m spatial resolution.

Tseng et al. [44] used Landsat-4/-5/-7/-8 Thematic Mapper (TM)/Enhanced TM Plus/Operational Land Imager imageries to reconstruct the topography of a tidal flat, to unveil its formation and temporal changes since the 1980s. They classified water areas by applying a modified normalized difference water index to each Landsat image and normalized the chances of water exposure to create an inundation probability map. After building DEM at the intertidal zone, a water level-area curve is established, and the accuracy of DEM is validated by sea level (SL) at the timing of each Landsat snapshot.

Since there is no simple method exists for mapping tidal flats over large (>1000 km) extents, and consequently, their global status and distribution remain poorly understood. Existing mapping methods are restricted to small areas with known tidal regimes because tidal flats are only fully exposed for a brief period around low tide. Murray et al. [45] proposed a method for mapping tidal flats over very large areas and demonstrated its utility by mapping the tidal flats of China, the Democratic People's Republic of Korea, and the Republic of Korea. They generated tide height predictions at the acquisition time of all Landsat Archive images of the study area using a validated regional tide model, selected suitable images acquired in the upper and lower 10% of the tidal range, converted high and low tide images to a land and water class image derived from the normalized difference water index (NDWI) and, subtracted the high tide classified image from the low tide classified image, resulting in the delineation of the tidal flat.

7. Conclusions

Land is the most precious resource for human life and sustainable development, which provides food, economic development environment, and healthy ecosystems for all organisms on Earth. Human activities have a significant impact on land use and its change from time to time. In this paper, the spatial-temporal land-use change characteristics of the coastal plains in Hangzhou Bay Area, China, were investigated. The driving force of land-use change was analyzed by investigating factors such as demographics and human population dynamics, social-economic development, urbanization, and coupling effects of the above-mentioned factors. The results presented in this paper can provide useful indicators and insights for environmental ecology evaluation and decision-making in coastal plain areas.

The objective of this study was to classify land-use and land-cover status and to identify land-use changes, especially the land-use distribution, land-use intensity, land-use change rate, and its driving force of the coastal plains in Hangzhou Bay Area in the past 12 years from 2009 to 2020. Satellite imageries and medium-scale Landsat data were used to extract information on land use and land-use changes. A random-forest-based land-use/land-cover classification system was established. Based on the fast, efficient, and parallel online computing function of GEE, this study uses multi-temporal Landsat series image data to classify and calculate the land-use characteristics of the study area in the most recent 12 years. Based on GIS technology, the change characteristics and spatial differences of land-use distribution and intensity were discussed, and the direction and rate of land-use change were analyzed. The impact of human activities on landscape is mainly reflected in agricultural production and urban construction activities.

Since the beginning of the 21st century, China's large-scale tidal flat land development has promoted the rapid development of the regional economy. The newly added land is mainly used for urbanization, industrialization, and port construction. The land-use mode of the coastal tidal flat has gradually changed from a natural state to an artificial mode, and the transformation rate is accelerating. While accelerating the development of ports and cities and the industrialization of coastal areas, coastal tidal flats also bring many land-based pollutants, and the water environment is not optimistic.

The results presented in this paper can provide useful indicators and insights for environmental ecology evaluation and decision-making in coastal plain areas. Ensuring the rational development and utilization of land resources is a necessary condition for realizing the sustainable development of the economy, society, ecological environment, and natural resources. With the rapid development of China's economy and society and the vigorous promotion of urbanization, the population density of coastal plain has been increasing continuously, and a series of problems such as ecological environment destruction and water shortages have emerged. A reasonable analysis of the response relationship between land-use function change and related ecological environment factors is of great significance for rational and efficient land-use planning.

Author Contributions: Y.Z. and R.A. conceived the idea and designed the algorithms. N.X. validated the modeling, D.O. and C.J. implemented the software modules. All authors have read and agreed to the published version of the manuscript.

Funding: This research was funded by the Basic Scientific Research Funds Program of Zhejiang Tongji Vocational College of Science and Technology (Grant No. FRF21PY002).

Data Availability Statement: Not applicable.

Conflicts of Interest: The authors declare no conflict of interest.

References

1. Haruyama, S. Landform and Vulnerability for Disaster in Land Use Changing. In *Natural Disaster and Coastal Geomorphology*; Haruyama, S., Sugai, T., Eds.; Springer: Cham, Switzerland, 2016. [CrossRef]

2. Hanks, R.D.; Baldwin, R.F.; Folk, T.H.; Wiggers, E.P.; Coen, R.H.; Gouin, M.L.; Agha, A.; Richter, D.D.; Fields-Black, E.L. Mapping Antebellum Rice Fields as a Basis for Understanding Human and Ecological Consequences of the Era of Slavery. *Land* **2021**, *10*, 831. [CrossRef]
3. Lambin, E.F.; Meyfroidt, P. Global land use change, economic globalization, and the looming land scarcity. *Proc. Natl. Acad. Sci. USA* **2011**, *108*, 3465–3472. [CrossRef]
4. Kim, J.-H.; Kwon, O.-S.; Ra, J.-H. Urban Type Classification and Characteristic Analysis through Time-Series Environmental Changes for Land Use Management for 31 Satellite Cities around Seoul, South Korea. *Land* **2021**, *10*, 799. [CrossRef]
5. Regasa, M.S.; Nones, M.; Adeba, D. A Review on Land Use and Land Cover Change in Ethiopian Basins. *Land* **2021**, *10*, 585. [CrossRef]
6. Richey, J.E.; Ballester, M.V.; Davidson, E.A.; Johnson, M.S.; Krusche, A.V. Land–Water interactions in the amazon. *Biogeochemistry* **2011**, *105*, 1. [CrossRef]
7. Gong, P.; Wang, J.; Yu, L.; Zhao, Y.; Zhao, Y.; Liang, L.; Niu, Z.; Huang, X.; Fu, H.; Liu, S.; et al. Finer Resolution Observation and Monitoring of Global Land Cover: First Mapping Results with Landsat TM and ETM+ Data. *Int. J. Remote Sens.* **2013**, *34*, 2607–2654. [CrossRef]
8. Rd El-kawy, J.; Ismail, H.; Suliman, A. Land use and land cover change detection in the western Nile delta of Egypt using remote sensing data. *Appl. Geog.* **2011**, *31*, 483–494. [CrossRef]
9. Leifeld, J. Prologue paper: Soil carbon losses from land-use change and the global agricultural greenhouse gas budget. *Sci. Total Environ.* **2013**, *465*, 3–6. [CrossRef] [PubMed]
10. Tiwari, P. Land use changes in Himalaya and their impacts on environment, society and economy: A study of the Lake Region in Kumaon Himalaya. *India. Adv. Atmos. Sci.* **2008**, *25*, 1029. [CrossRef]
11. Kanga, E.M.; Ogutu, J.O.; Piepho, H.-P.; Olff, H. Human–hippo conflicts in Kenya during 1997–2008: Vulnerability of a megaherbivore to anthropogenic land use changes. *J. Land Use Sci.* **2011**, *7*, 395–406. [CrossRef]
12. Drummond, M.A.; Loveland, T.R. Land-use Pressure and a Transition to Forest-cover Loss in the Eastern United States. *BioScience* **2010**, *60*, 286–298. [CrossRef]
13. Wang, C.; Gao, Q.; Wang, X.; Yu, M. Spatially differentiated trends in urbanization, agricultural land abandonment and reclamation, and woodland recovery in Northern China. *Sci. Rep.* **2016**, *6*, 37658. [CrossRef] [PubMed]
14. Rawat, J.; Kumar, M. Monitoring land use/cover change using remote sensing and GIS techniques: A case study of Hawalbagh block, district Almora, Uttarakhand, India. *Egypt. J. Remote. Sens. Space Sci.* **2015**, *18*, 77–84. [CrossRef]
15. Wang, J.; Li, C.; Hu, L.; Zhao, Y.; Huang, H.; Gong, P. Seasonal land cover dynamics in Beijing derived from Landsat 8 data using a spatio-temporal contextual approach. *Remote. Sens.* **2015**, *7*, 865–881. [CrossRef]
16. Landsat 7 SLC Gap-Filled Products Phase One Methodology. Available online: https://www.usgs.gov/media/files/landsat-7-slc-gap-filled-products-phase-one-methodology (accessed on 15 October 2021).
17. Lee, J.S.H.; Wich, S.; Widayati, A.; Koh, L.P. Detecting industrial oil palm plantations on Landsat images with Google Earth Engine. *Remote Sens. Appl. Soc. Environ.* **2016**, *4*, 219–224. [CrossRef]
18. Huang, H.; Zhou, Y.; Qian, M.; Zeng, Z. Land Use Transition and Driving Forces in Chinese Loess Plateau: A Case Study from Pu County, Shanxi Province. *Land* **2021**, *10*, 67. [CrossRef]
19. Chai, Y.; Qiao, W.; Hu, Y.; He, T.; Jia, K.; Feng, T.; Wang, Y. Land-Use Transition of Tourist Villages in the Metropolitan Suburbs and Its Driving Forces: A Case Study of She Village in Nanjing City, China. *Land* **2021**, *10*, 168. [CrossRef]
20. El-Hamid, H.T.A.; Caiyong, W.; Yongting, Z. Geospatial analysis of land use driving force in coal mining area: Case study in Ningdong, China. *GeoJournal* **2021**, *86*, 605–620. [CrossRef]
21. Teixeira, Z.; Teixeira, H.; Marques, J.C. Marques, Systematic processes of land use/land cover change to identify relevant driving forces: Implications on water quality. *Sci. Total Environ.* **2014**, *470–471*, 1320–1335. [CrossRef]
22. Zhou, Y.; Li, X.; Liu, Y. Land use change and driving factors in rural China during the period 1995-2015. *Land Use Policy* **2020**, *99*, 105048. [CrossRef]
23. Meshesha, T.W.; Tripathi, S.K.; Khare, D. Analyses of land use and land cover change dynamics using GIS and remote sensing during 1984 and 2015 in the Beressa Watershed Northern Central Highland of Ethiopia. *Model. Earth Syst. Environ.* **2016**, *2*, 168. [CrossRef]
24. Kleber, M.; Bourg, I.C.; Coward, E.K.; Hansel, C.M.; Myneni, S.C.B.; Nunan, N. Dynamic interactions at the mineral–organic matter interface. *Nat. Rev. Earth Environ.* **2021**, *2*, 402–421. [CrossRef]
25. Zhang, C.; Sargent, I.M.J.; Pan, X.; Li, H.; Gardiner, A.; Hare, J.; Atkinson, P.M. Atkinson, Joint Deep Learning for land cover and land use classification. *Remote Sens. Environ.* **2019**, *221*, 173–187. [CrossRef]
26. Zou, Y.; Greenberg, J.A. A spatialized classification approach for land cover mapping using hyperspatial imagery. *Remote Sens. Environ.* **2019**, *232*, 111248. [CrossRef]
27. Marcos, D.; Volpi, M.; Kellenberger, B.; Tuia, D. Land cover mapping at very high resolution with rotation equivariant CNNs: Towards small yet accurate models. *ISPRS J. Photogramm. Remote Sens.* **2018**, *145*, 96–107. [CrossRef]
28. Srivastava, S.; Vargas-Muñoz, J.E.; Tuia, D. Understanding urban land use from the above and ground perspectives: A deep learning, multimodal solution. *Remote Sens. Environ.* **2019**, *228*, 129–143. [CrossRef]
29. Pan, X.; Zhang, C.; Xu, J.; Zhao, J. Simplified object-based deep neural network for very high resolution remote sensing image classification. *ISPRS J. Photogramm. Remote Sens.* **2021**, *181*, 218–237. [CrossRef]

30. Rozenstein, O.; Karnieli, A. Comparison of methods for land-use classification incorporating remote sensing and GIS inputs. *Appl. Geog.* **2011**, *31*, 533–544. [CrossRef]
31. Gorelick, N.; Hancher, M.; Dixon, M.; Ilyushchenko, S.; Thau, D.; Moore, R. Google Earth Engine: Planetary-scale geospatial analysis for everyone. *Remote Sens. Environ.* **2017**, *202*, 18–27. [CrossRef]
32. Hansen, M.C.; Potapov, P.V.; Moore, R.; Hancher, M.; Turubanova, S.A.; Tyukavina, A.; Thau, D.; Stehman, S.V.; Goetz, S.J.; Townshend, J.R.G.; et al. High-Resolution Global Map of 21st-Century Forest Cover Change. *Science* **2013**, *342*, 850–853. [CrossRef]
33. Liu, X.; Hu, G.; Chen, Y.; Li, X.; Xu, X.; Li, S.; Pei, F.; Wang, S. High-resolution multi-temporal mapping of global urban land using Landsat images based on the Google Earth Engine Platform. *Remote Sens. Environ.* **2018**, *209*, 227–239. [CrossRef]
34. Ji, L.; Gong, P.; Geng, X.; Zhao, Y. Improving the Accuracy of the Water Surface Cover Type in the 30 m FROM-GLC Product. *Remote Sens.* **2015**, *7*, 13507–13527. [CrossRef]
35. Xulu, S.; Phungula, P.T.; Mbatha, N.; Moyo, I. Multi-Year Mapping of Disturbance and Reclamation Patterns over Tronox's Hillendale Mine, South Africa with DBEST and Google Earth Engine. *Land* **2021**, *10*, 760. [CrossRef]
36. Randazzo, G.; Cascio, M.; Fontana, M.; Gregorio, F.; Lanza, S.; Muzirafuti, A. Mapping of Sicilian Pocket Beaches Land Use/Land Cover with Sentinel-2 Imagery: A Case Study of Messina Province. *Land* **2021**, *10*, 678. [CrossRef]
37. Terres de Lima, L.; Fernández-Fernández, S.; Gonçalves, J.F.; Magalhães Filho, L.; Bernardes, C. Development of Tools for Coastal Management in Google Earth Engine: Uncertainty Bathtub Model and Bruun Rule. *Remote Sens.* **2021**, *13*, 1424. [CrossRef]
38. Teluguntla, P.; Thenkabail, P.; Oliphant, A.; Xiong, J.; Gumma, M.K.; Congalton, R.G.; Yadav, K.; Huete, A. A 30-m landsat-derived cropland extent product of Australia and China using random forest machine learning algorithm on Google Earth Engine cloud computing platform. *ISPRS J. Photogramm. Remote Sens.* **2018**, *144*, 325–340. [CrossRef]
39. Wingate, V.R.; Phinn, S.R.; Kuhn, N.; Bloemertz, L.; Dhanjal-Adams, K.L. Mapping decadal land cover changes in the woodlands of northeastern Namibia from 1975 to 2014 using the Landsat satellite archived data. *Remote Sens.* **2016**, *8*, 681. [CrossRef]
40. Chan, J.C.-W.; Paelinckx, D. Evaluation of Random Forest and Adaboost tree-based ensemble classification and spectral band selection for ecotope mapping using airborne hyperspectral imagery. *Remote Sens. Environ.* **2008**, *112*, 2999–3011. [CrossRef]
41. Pelletier, C.; Valero, S.; Inglada, J.; Champion, N.; Dedieu, G. Assessing the robustness of Random Forests to map land cover with high resolution satellite image time series over large areas. *Remote Sens. Environ.* **2016**, *187*, 156–168. [CrossRef]
42. Schmidt, M.; Pringle, M.; Devadas, R.; Denham, R.; Tindall, D. A framework for large-area mapping of past and present cropping activity using seasonal Landsat images and time series metrics. *Remote Sens.* **2016**, *8*, 312. [CrossRef]
43. Wang, X.; Xiao, X.; Zou, Z.; Chen, B.; Ma, J.; Dong, J.; Doughty, R.; Zhong, Q.; Qin, Y.; Dai, S.; et al. Tracking annual changes of coastal tidal flats in China during 1986–2016 through analyses of Landsat images with Google Earth Engine. *Remote Sens. Environ.* **2020**, *238*, 110987. [CrossRef] [PubMed]
44. Tseng, K.-H.; Kuo, C.-Y.; Lin, T.-H.; Huang, Z.-C.; Lin, Y.-C.; Liao, W.-H.; Chen, C.-F. Reconstruction of time-varying tidal flat topography using optical remote sensing imageries. *ISPRS J. Photogramm. Remote Sens.* **2017**, *131*, 92–103. [CrossRef]
45. Murray, N.J.; Phinn, S.R.; Clemens, R.S.; Roelfsema, C.M.; Fuller, R.A. Continental Scale Mapping of Tidal Flats across East Asia Using the Landsat Archive. *Remote Sens.* **2012**, *4*, 3417–3426. [CrossRef]